3D PRINTED POLY-LACTIC ACID FOR PARTIAL DISCHARGE STUDIES

by

PUNEET GILL

A thesis submitted to the Faculty of Graduate Studies of

The University of Manitoba

In partial fulfillment of the requirements for the degree of

MASTER OF SCIENCE

Department of Electrical and Computer Engineering

University of Manitoba

Winnipeg, Manitoba, Canada

Abstract

The electric and power industry is moving towards environmentally sustainable components and systems. A significant step towards achieving these goals is developing environmentally friendly insulation materials. Initially, polymers replaced natural insulation materials and have dominated the electrical insulation industry for a long time. For years, the management and disposal of synthetic insulation material have been a concern, thereby contributing to environment pollution. Biopolymers represent a potential solution to this ecological problem. Poly lactic acid (PLA) is one such biopolymer with properties comparable to the polymers used in electrical insulation. In this study, PLA samples were designed, and 3D printed to have a void (i.e., air cavity) in order to conduct partial discharge studies. The physical characteristics and dielectric properties of the samples were analyzed. In addition, x-ray microtomography was performed on the samples before continuing with the partial discharge experiment, providing a non-destructive and quantitative method for characterizing the samples. Three-dimensional x-ray microtomography scans and phase resolved partial discharge patterns for the samples are presented in support of the conclusions. This work provides a basis for more detailed investigations of material degradation due to partial discharge.

Acknowledgements

I would like to express my gratitude and appreciation to my advisor Dr. Derek Oliver for his guidance and support throughout my course work, research, and writing. His persistent help and assistance are the reason this dissertation is ready. I would also extend my gratitude to Dr. Behzad Kordi, and Dr. Jason Morrison for their time and effort in the laboratory work.

I wish to acknowledge the financial assistance provided by the Natural Sciences and Engineering Research Council (NSERC), the Faculty of Graduate Studies (FGS) and the Manitoba Institute for Materials (MIM) at the University of Manitoba.

I would like to express my sincere appreciation to my colleagues in the Department of Electrical and Computer Engineering, the Department of Biosystems Engineering, the Price Faculty of Engineering, and the Manitoba Institute of Materials for their constant help in the lab work.

Last, I am grateful to my mother Baljinder Gill for her constant support and encouragement. I am also, thankful to my family and friends for always being there for me.

To my parents Baljinder and Jaswinder Gill

TABLE OF CONTENTS

List of Figures

List of Tables

CHAPTER 1

INTRODUCTION

1.1 Objective

This thesis aims to assist the development of biopolymers for electrical insulation applications focusing on the material poly lactic acid (PLA). The thesis explains the fabrication process and material properties of PLA by additive manufacturing and the dielectric properties and effects of partial discharge on the sample. In particular this thesis demonstrates that PLA may be used to fabricate samples suitable for fundamental studies of partial discharge detection and its impact on the materials within which the partial discharge occurs.

The fabrication of a cylindrical PLA sample includes design, selecting efficient printer settings, and printing the sample. Multiple samples were printed – PLA disc samples, PLA cylindrical control samples and cylindrical samples with a void at the center along the vertical rotational axis of the cylinder.

The dielectric properties of these samples were primarily analysed using a *Solartron* Dielectric-spectroscope. To better understand the fabrication results, samples with varying

dimensions were designed, printed, and studied under x-ray microtomography. Finally, partial discharge (PD) signatures were obtained from several samples.

1.2. Biopolymers as Electrical Insulation Material

Cross-linked polyethylene and related materials are commonly used as electrical insulation materials. Still, these are not ecologically friendly as their inherent longevity (in terms of service lifetime) points to their resistance to break down/degrade once their service is completed. This delayed degradation contributes to a many ecological challenges, including groundwater contamination and the presence of micro-plastics in food chains. In response to this, eco-friendly materials such as biodegradable polymers are considered potential replacements [1]. The biodegradable polymer in focus in this thesis is polylactic acid (PLA). Some studies have suggested that PLA has better clarity, strength, rigidity, thermal resistance, and dimensional stability than other biodegradable polymer films [2]. Other candidate materials such as polyhydroxyalkanoates (PHA), polyhydroxybutyrate (PHB) and 3-hydroxybutyrate-co-3-hydroxyvalerate (PHBV) are also in consideration [3], but their properties are beyond the scope of this study.

1.3 Contributions

This thesis builds on previous studies of biodegradable polymers, particularly poly lactic acid (PLA) as applied to the problem of electrical insulation. This study culminates in the first documented partial discharge study on employing 3D printed PLA samples that contain voids and demonstrates how to non-destructively and quantitatively characterize the void size and geometry. Before the partial discharge measurements, x-ray microtomography was performed to understand

the fabrication process of the samples better. Multiple samples were fabricated, and their physical characteristics were analysed by atomic force microscopy, optical microscopy, and profilometry. The dielectric properties of the PLA samples were measured and found to be comparable to data in literature. With the analysis and better understanding of additive manufacturing process and the partial discharge behaviour of PLA samples, this thesis forms a substantial base for future work.

1.4. Thesis Outline

Chapter 1: Introduction to this thesis explaining the objective of the research and an overview of application of biopolymers as electrical insulation materials.

Chapter 2: History of materials used for high voltage insulation. Discussion of sample fabrication techniques and their advancement to most recent additive manufacturing over the years. A Literature review of solid polymeric material and an introduction of partial discharge in cable insulation - types and models.

Chapter 3: Describing the material under investigation during the research – PLA; its fabrication process, material properties and limitations. Moreover, a report of the physical characterization techniques applied to the given samples- optical microscopy, atomic force microscopy and profilometry. An explanation of the dielectric properties of PLA observed while conducting dielectric spectroscopy on the sample. X-ray Microtomography on the samples to understand the inner structure of the 3D printed sample before performing partial discharge experiments on the samples.

Chapter 4: Analysis of the results collected during the duration of the research. Observations from the physical characteristic of the sample – topographical analysis using atomic force microscopy.

Dielectric properties from the dielectric spectroscopy and results from partial discharge experiments performed on samples with single and multiple voids.

Chapter 5: Conclusion of the thesis including the main finding from the experiments performed on the PLA sample – x-ray microtomography and partial discharge experiment, that could potentially extend and be beneficial to future research on PLA and other 3D-printable systems.

Chapter 2

Literature Review

2.1 Insulation Materials for High Voltage Applications

At the beginning of the 20th century, the primary insulation materials used were derived from natural materials, including asphalt, mica, rubber, cotton thread, and fabric [4]. These naturally sourced insulation materials had many shortcomings, particularly limited breakdown strength and/or limited withstand capabilities. The search for better insulation materials have been driven by the need to transmit power at higher voltages and the desirability of more compact, lighter and longer-lasting alternatives to natural materials. Nevertheless, there are still a few highly effective and yet widely used natural materials such as glass and porcelain. Some of these materials are noteworthy as they have been in service for many decades and continue to meet or exceed installation requirements.

Polyvinylchloride (PVC) initially replaced natural rubber as underground cable insultation and house wiring. But PVC was limited to low voltage application despite advances in the compounding of polyvinylchloride (PVC) [4]. Since the 1960s, the range of synthetic insulation

material options and use have grown replacing natural insulating materials in the power cable industry as there were limited naturally sourced materials available for high voltage applications. It was during the 1960s that extruded polyethylene was introduced for use in high voltage cables, replacing oil-impregnated paper in 13 kV and 23 kV underground residential cables [5]. The extruded polyethylene had the added benefit of reducing manufacturing, and installation costs, increasing the service reliability of splices. In 1963, shortly after the widespread adoption of polyethylene, cross-linked polyethylene (XLPE) found application in medium voltage cables. The benefits of XLPE, when compared to polyethylene, include improved mechanical and thermal properties.

To further enhance the electrical properties of these synthetic materials, plasticizers, fillers, and stabilizers have been added. These additives broaden the range of material properties accessible by the base polymer and, in turn, the range of applications in which it can be employed.

Following the advancements in XLPE production, ethylene propylene rubber (EPR) was developed and substituted for natural rubber, which was still the most frequently used insulation material for high voltage applications. EPR based insulation power cables were immediately used at a transmission voltage of 138 kV as EPR does not require moisture protection until 138 kV. Beyond this operating voltage, the insulation requires additional protection in the form of a metallic moisture barrier [6].

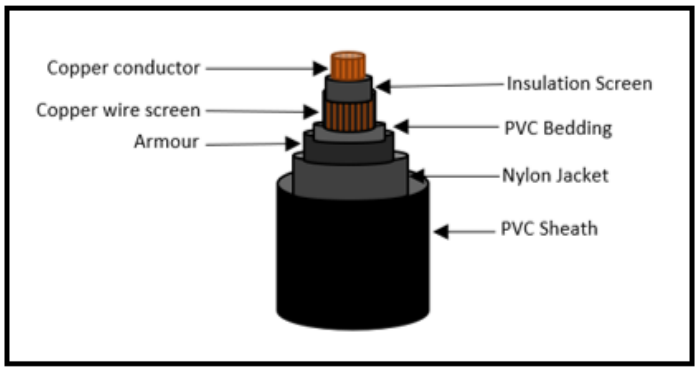

Figure 2.1. Cross-section of an electrical power cable

Insulating materials can be classified into three main categories based on their chemical composition: inorganic insulating materials, polymeric organic materials, and composite insulating materials [7] as summarized in Table 2.1. Inorganic materials such as glass and porcelain have high densities, enabling them to withstand high temperatures. They are generally highly chemical resistant but are difficult to machine as these materials are brittle. This lack of flexibility- means that they have limited-service locations and are prone to physical failure. They can be manufactured to have highly hydrophobic surfaces, but the quality of these can be compromised by weathering in service which, in turn, significantly reduces their service performance. Polymeric organic materials, on the other hand, have low density, are generally hydrophobic (or can be designed to have hydrophobic surfaces) and are compact.

Table 2.1: Classification of High Voltage Insulating Materials on basis of their composition [7]

Types	**Materials**
Inorganic Insulating Materials	Ceramic Insulating Materials, Glass, fiberglass, enamel, mica and asbestos.
Polymeric Organic Materials	Thermoplastic polymers (polyethylene, polyvinylchloride, polypropylene, and polyamide), Thermoset plastics (polyester-resin, phenol-resin, epoxy resin) and poly compounds.
Composite Insulating system	Impregnated paper, fiber reinforced plastics and insulation board material

The increased use of synthetic insulation material over the 20th century has provided some of the incentive to develop bio-degradable polymers. Although synthetic materials have some advantages over natural materials, the management and disposal of synthetic materials have continued to be a question for discussion [8]. The desire to consider the effect on the environment in producing and disposing of electrical wires and cables [9] has kindled interest in using bio-degradable polymers. These are polymers that the action of microorganisms can decompose into their component elements.

Biopolymers have gained popularity in the last three decades as materials that could be easily decomposed into a beneficial form for the environment. Biopolymers like microbial polyhydroxyalkanoates (PHAs, PLA and PHBV) are promising polymers which would help reduce the environmental burden of petroleum-derived polymers.

2.2 Additive Manufacturing of Plastic Materials

Additive manufacturing uses digitally controlled and operated material laying tools to achieve advantages over conventional (subtractive) manufacturing methods such as milling, injection casting or high-pressure casting, plastic, or metal foaming [10]. Additive manufacturing presents an integrated design-manufacturing approach to process plastic that has potential application in the aerospace, medical, and automotive industries [11].

The fabrication process of additive manufacturing implies constructing a 3D physical object from digital models through layer-by-layer deposition of material such as plastic, metal, or ceramic [12]. Before the object is "printed," a three-dimensional design file is made using computer-aided design (CAD) based on finite element simulation of the printing process [13]. A design file is created, which is translated into instruction for the "printer", and this translated file produces a secondary set of files with codes that instructs the "printer". Additive manufacturing technology is gaining traction as an alternative because of the flexibility and adaptability compared to the traditional manufacturing process through versatility in design and decreased costs due to the reduction in tooling requirements [13]. Potential benefits of additive manufacturing include a direct translation from design to a manufactured component without capacity for customization without being constrained by the manufacturing process. The greatest advantage is the product received is in a near-final state, having been produced quickly and at a low manufacturing cost [14].

In response to the growth in additive manufacturing, ASTM International (in ASTM 52900:2015) [13] has defined seven categories of this new technology: binder jetting (BJ); directed energy deposition (DED); material extrusion (ME); material jetting (MJ); powder bed fusion

(PDF); sheet lamination (SL); and vat photopolymerization (VP) [12,13] which are summarized in Table 2.2.

Table 2.2: Basic Principles and Materials associated with the ASTM categorization of additive manufacturing [13]

ASTM	Principle	Technology	Materials
Binder Jetting (BJ)	Liquid binders jet printed onto a thin layer of powder. Built up by gluing the particles together layer by layer	3D Inkjet Technology	Polymers, Ceramics, Composites, Metals and Hybrid
Directed Energy Deposition (DED)	Focused thermal energy melts materials during deposition and adds material alongside the heat input. It often has an inert gas blown together with powder from nozzles.	Laser deposition, Electron beam plasma arc melting.	Metals and Hybrids
Material Extrusion (ME)	Material is extruded through a nozzle	Fused Deposition Modelling and Fused Layer Modelling	Polymer and Composites
Material Jetting (MJ)	Droplets of build material are deposited could be hot and cold – cold spray jetting relies on the high speed of the small particles of material, the energy to fuse/deposit comes from the loss of kinetic energy as the particle impacts the target.	3D Inkjet technology and Direct Ink writing	Polymer, Ceramics, Composites Hybrid
Powder bed fusion (PBF)	Thermal energy (laser or electron beam) is used to melt and fuse a material powder together. PBF require the spreading of the powder material over previous layers.	Electron beam melting, Direct Metal Laser Sintering and Selective Laser Melting/Sintering	Metals, Ceramics, Polymers, Composites and Hybrid
Sheet Lamination (SL)	Thin sheets of material are bonded together layer by layer to form a single piece that is cut into 3D object.	Laminated Object Manufacturing, Ultrasound Additive Manufacturing.	Polymers, Metals, Ceramics and Hybrids
Vat Photopolymerization (VP)	Liquid polymer in a vat is cured/hardened under ultra-violet light	Stereo Lithography (STL) and Digital Light Processing (DLP)	Polymer and Ceramics

As a result, depending on the printing method and the material to be printed, objects are fabricated by extruding material from the extruder in a successive layer-by-layer fashion.

2.3 Partial Discharge

Cable insulation plays a crucial role in a power system network; an insulation failure can impact the transmission line and cause lengthy outages for end users. Therefore, it is essential to maintain the continuity of power and detect any developing fault in a power cable [15].

2.3.1 Types of Partial Discharge

Partial discharge can occur in solids, liquids, and gases and can be divided mainly into internal discharge, surface discharge, and corona discharge. Internal discharges occur when partial discharges occur in cavities within a solid or liquid dielectric system. In solids, this type of partial discharge is unavoidable as the holes are formed during the manufacturing process. The second type of partial discharge is a surface discharge, which occurs at the air- interface of a liquid or a solid dielectric. Surface discharges are observed when the electric field component parallel to the interface becomes extremely high [16]. Corona discharge occurs around a conductor that is energized to a high voltage, which causes local ionization of the surrounding air. As corona discharge results from local ionization, the ambient pressure and humidity are influential factors. Corona discharge is often accompanied by noise and a visible glow of light in the dark.

2.3.2 Partial Discharge Sensors

The observation of partial discharges is a crucial consideration in the integrity assessment of the cables. Long-term partial discharges are associated with deterioration within the insulation and a corresponding loss of reliability. Partial discharge tests are a component of the quality assurance testing carried out on cables during manufacturing to check for manufacturing defects. They are also carried out on cables while in-service to detect insulation deterioration in the cables. Formally, Partial Discharge is defined in IEC 60270 [17] (Partial discharge measurements) as "a localised electrical discharge that partially bridges the insulation between conductors and which may or may not occur adjacent to a conductor" [18].

The presence of partial discharges can represent the dielectric breakdown within a section of a dielectrically- stressed insulation path due to a void or crack [19]. This discharge produces varying signals which travel in the cable and are attenuated and dispersed in the cable conductor. Different partial discharge sensing techniques are used to capture this signal in a cable, including capacitive/inductive couplers, and acoustic emission techniques [18]. In the first of these, a coupling capacitor is placed parallel to the test object and discharge signals are measured across external impedance involving a resonant circuit. It is difficult to perform field measurements of partial discharge as traditional methods can only detect partial discharges in short, and isolated cable lengths [20]. Inductive coupling only records the partial discharges that cause current to go through inductive coupling unlike capacitive coupling, which records discharge for the whole cable. Inductive coupling is more suitable for on-site partial discharge measurements for MV cables [21]. The acoustic partial discharge detection technique detects the mechanical signal emitted from the discharge. The onset of a partial discharge appears like a small explosion which

excites a mechanical wave that propagates through the insulation and is detected with an acoustic technique [22]. The partial discharge causes fast rising pulses that appear as short bursts in cables that partial discharge sensors can detect. Using the IEC 60270 [17] approach, the apparent PD magnitude is obtained from the accumulated magnitude of these pulses as measured by a high frequency current transformer and associated equipment [23].

2.3.3 Partial Discharge Models

Four major partial discharge models are commonly used to represent the cavity-dielectric system: the three-capacitance or the abc-model; the induced charge concept (ICC); the multiphysics model; and finite element analysis (FEA).

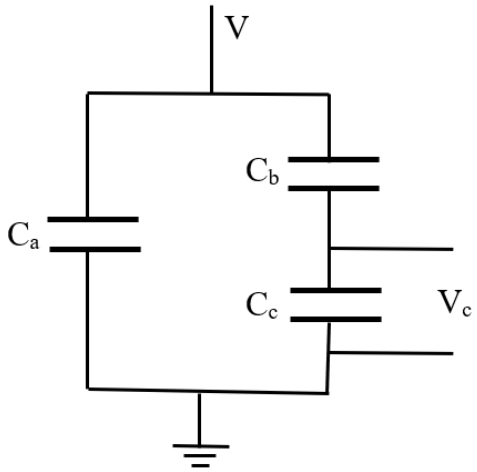

Figure 2.2: Equivalent circuit of the three capacitance (abc) model

The abc model uses an equivalent circuit including three capacitances to model the cavity, the insulation in series with cavity (Figure 2.2) where C_a is parallel capacitance, C_b is series capacitance, C_c void capacitance and V_c is the voltage across the void. Equation (1) shows the value of V_c before PD occurs, equation (2) is PD apparent charge, and equation (3) is the real charge, where ΔV is the voltage reduction across the void due to the discharge [24].

V_c before PD occurs equals to: $V_C = \frac{C_b}{C_b + C_c}$ (1)

PD apparent charge: $q_{app} = C_b \Delta V$ (2)

Real charge: $q_{real} = \left[C_c + \frac{C_a C_b}{C_a + C_b} \right] \Delta V$ (3)

The induced charge concept is an analytical method to explain the partial discharge transient [25, 26]. The induced charge model is based on the charge distribution on the void surface due to discharge; these charges are from an electric dipole configuration that induces charges on the electrode [24]. Multiphysics models require a high number of physical parameters that must be determined experimentally. These physical parameters are a combination of simulation results and measurement results. The success of Multiphysics approaches is tempered by the inability to generalize key parameters such as testing geometry and dimensions. These must be determined experimentally [27]. Finally, Finite Element Analysis is a numerical technique that can be applied to solve the partial differential equations associated with partial discharge models. The FEA approach combine statistical and other computational tools such as a finite difference models, finite element method and charge simulation method [27]. Using all of these, it is possible to numerically estimate the electric field intensity in the cavity-dielectric system.

In the last decade there have been studies of partial discharges that voids of different dimensions and shapes have been created (e.g., sphere, ellipsoids, and cubes) in cable insulation to better understand the impact of partial discharge on the cable insulation. It has been observed that under a non-uniform distribution of electric field in a void and insulation, the occurrence of per cycle partial discharge is higher under higher applied voltage and larger size of void [18]. It

has also been observed that partial discharge characteristics such as inception level, magnitude and repetition rate are all sensitive to the voids structure [28].

The most common reason for partial discharge in cables is voids and imperfections in the insulation. The voids would continue to exist, and the partial discharge occurring in those voids would enlarges their size, ultimately degrading the insulation's operational capabilities. Refinement of the techniques for detecting voids would help their earlier detection. By understanding the evolution of void degradation, this problem can be handled better.

Chapter 3:

Materials and Methods

3.1 Materials

This chapter provides documentation of the polymer samples designed, printed, and tested during this research. The material characteristics and design are a significant part of accessing the sample's dielectric properties and partial discharge analysis. The samples were all fabricated from PLA (poly- lactic acid) using 3D printers and ranged from thin disc samples to cylindrical samples of different dimensions, some of which had voids at the surface and others contained voids within the sample. The overall goal was to fabricate and analyze cylindrical samples with and without a void at the center of the sample's center. During the research, multiple samples were designed, and 3D printed with variations in the fabrication process depending on the observations made

while investigating. Additionally, experiments were performed on these samples to gain knowledge of the electrical properties of the material.

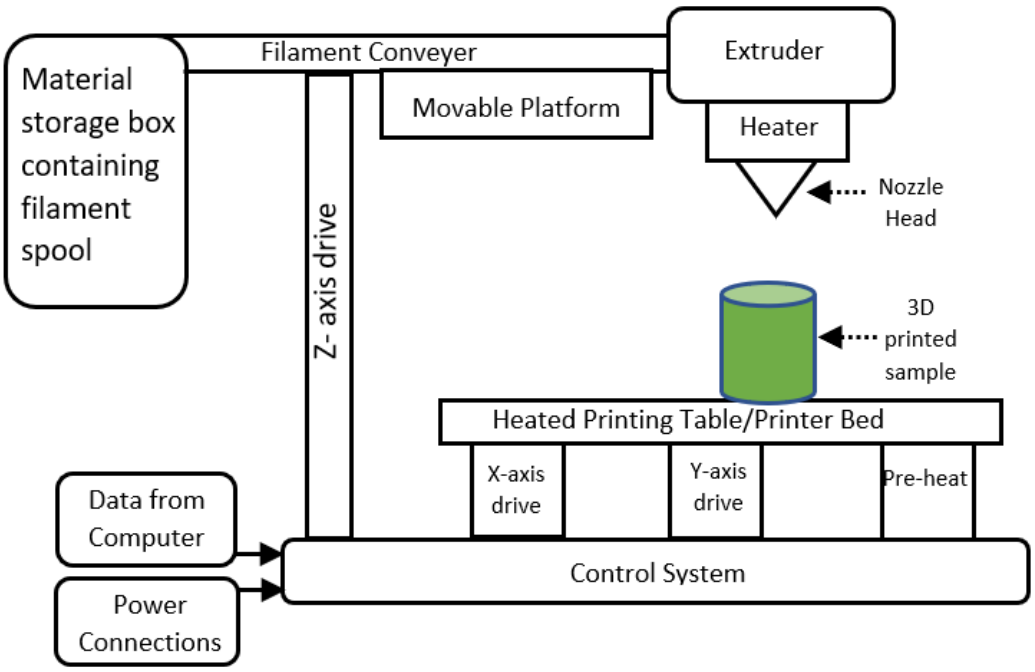

Figure 3.1. Standard diagram of a 3D Printer with multiple components including extruder, heater, a nozzle head, heated printer bed made by placing a glass plate over build plate (aluminum or steel) held together using build plate clamps, movable driver (XYZ axis) and connections with computer and power.

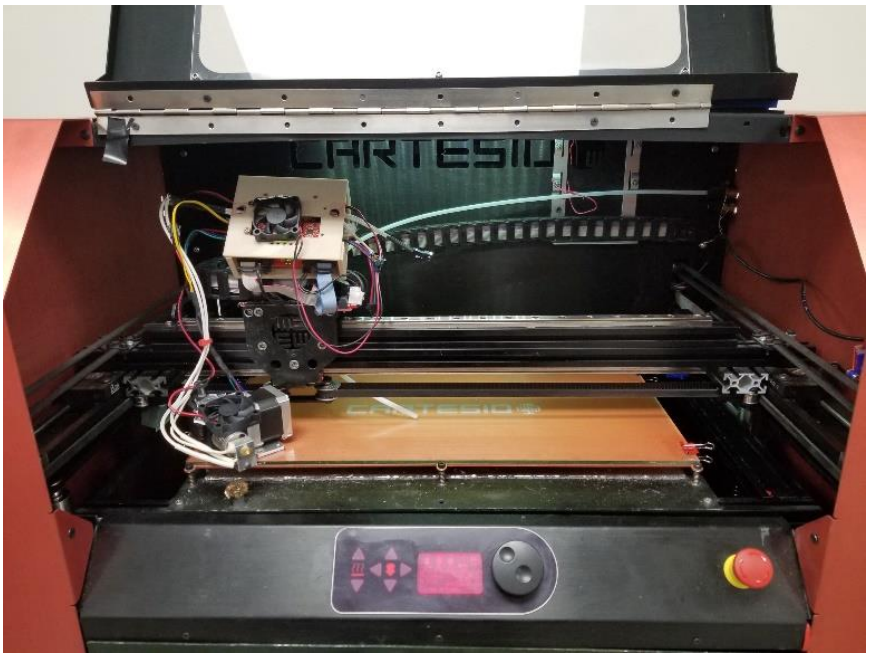

Figure 3.2: Image of the Cartesio v12 W 3D Printer manufactured by MAUK Custom Creations with multiple components including extruder, a nozzle head, heated printer bed and connections with computer and power.

The samples were printed using multiple 3D printers available at the University of Manitoba. An *Utlimaker-3 3D printer* was the first printer to be used, supported by *Ultimaker Cura* printing software. The *Ultimaker-3* printer operates with a nozzle temperature in the range 80 °C to 280 °C [29]. The other printer used was an *AXIOM Dual Extruder 3D Printer*. Supported by *APEX* printing software, this 3D-printer can operate with a maximum nozzle temperature of 315 °C [30]. The third printer *Cartesio v12 W* manufactured by *MAUK Custom Creations* operates at a nozzle temperature of 100 °C to 300 °C using Marlin firmware version 1.1.9.

3.1.1. PLA Discs

The first samples fabricated were PLA discs with 60 mm radius and thicknesses varying from 300 µm, 500 µm and 1000 µm. The discs were designed in the software *OpenSCAD*, to get

a three-dimensional computer aided design of the cylindrical disc. The design file created in *OpenSCAD* is obtained in the Standard Tessellation Language or Stereolithography (STL) file format. An STL file is used for prototyping and rendering purpose [31]. This STL design file was opened within the "slicer" software, chosen from those available: *Cura, PrusaSlicer* and *Repetier-Host*. The slicer operates on software defined default setting until the user defines the parameters for printing. Within the slicer software, the most suitable combination of printer settings was selected based on the material (PLA) and the dimension of the sample we are printing. One example of the print settings was choosing the "infill" as concentric circles for disc samples but *aligned rectilinear* for the cylindrical samples (Figure 3.3). Once these settings had been confirmed, the slicer software then produced a g-code file that was uploaded to the printer in order to print the three-dimensional sample.

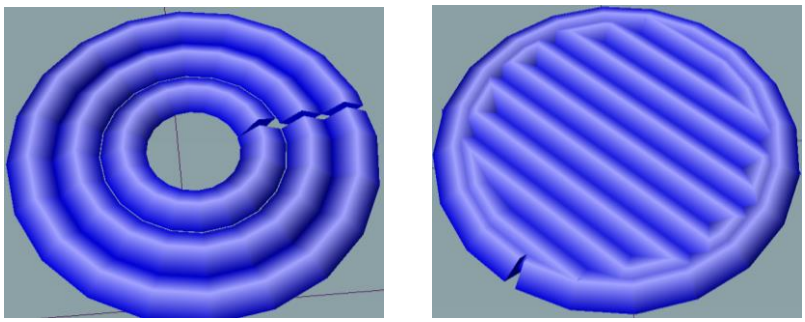

(a) (b)

Figure 3.3 Example of infill printer settings for single layer for disc and/or cylindrical samples (a) concentric circles (b) aligned rectilinear.

The fabrication process of a printed 3D sample uses multiple software elements, which creates discrepancies between the 3D printed sample and the original 3D design file. These arise from sources that include the operational limitations of the printer and the impact of storage

conditions such as age of the filament and the effect of ambient temperature and humidity on the source material.

The first PLA disc sample was printed using the *Cartesio v12 W* printer. The disc printed was 60 mm in diameter and 300 µm thick. The side of the disc that was in contact with the heated printer bed was smooth, but the opposite side was comparatively rough with print lines (tracks) that were visible to the naked eye (Figure 3.4).

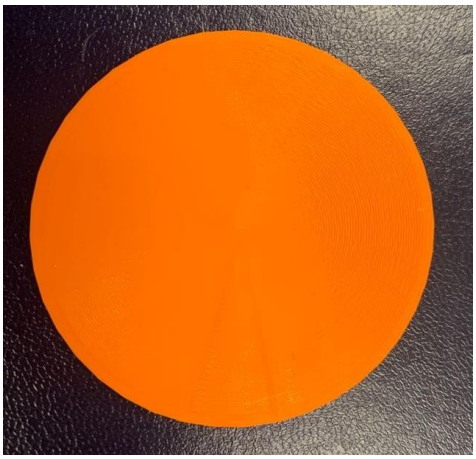

Figure 3.4: 3D printed PLA disc sample using infill setting as concentric by Cartesio v12 W printer

An optical microscope was used to provide initial characterization of the size/depth of the tracks. In an effort to get similar smooth surfaces on both sides of the disc, it was placed between aluminum metal plates inside an oven at 90 °C for 45 minutes (Figure 3.3(a)). Unfortunately, this did not smooth the disc surface and the disc itself appeared to warp, with noticeable deformation of the shape and thickness of the sample.

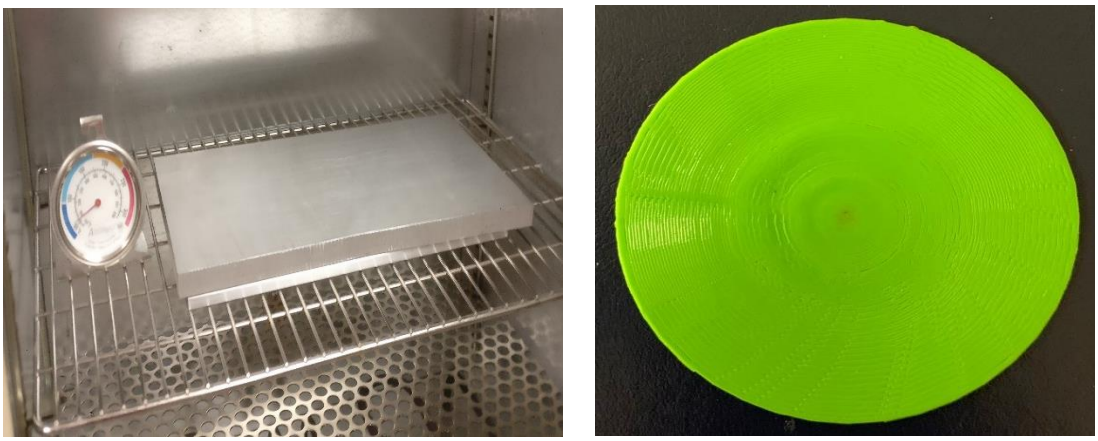

(a) (b)

Figure 3.5: (a) Heat treatment setup for compressing PLA discs between two aluminium plates at 90 °C in an oven. (b) Visible warps formed in the sample after heat treatment in the oven.

As an alternative, - the 'ironing' setting of the 3D printer was employed in an attempt to obtain smoother surface of the sample. In the process of *ironing* the hot extruder nozzle that guides the PLA filament runs over the sample slowly without extruding any filament on the surface during printing. By keeping the PLA softer for longer, a more even (smooth) finish can be expected. The surface roughness of the resulting PLA discs was characterized using an atomic force microscopy (AFM) and a surface profilometer. Furthermore, dielectric spectroscopy was performed on the samples to characterize the dielectric constant of the as-printed poly-lactic acid (PLA).

3.1.2. PLA Cylinders

The research objective is to use PLA biopolymer samples to provide a testing environment for fundamental studies of partial discharge generation from voids. Over time insulation materials develop voids/air gaps from which partial discharge occurs. Samples with voids and without voids (called control samples) were designed, to compare the amount of partial discharge observed for samples with different sizes of voids and control samples.

A set of cylindrical samples with a range of geometric structures were fabricated (Figure 3.6) to understand the accuracy of 3D printing and test to ensure the reliability of the printing process. It was performed to confirm whether the dimensionality of the samples would replicate the expected dimensions, and whether x-ray microtomography setup could quantitively measure these features. The samples were of external dimensions 10mm axial length and 12 mm diameter with internal surfaces shaped a hollow cylinder (inner diameter 6 mm), slanted hollow cylinder (axial length of shorter side 5 mm and inner diameter of 6 mm), a cone (cone depth 9 mm and diameter 6 mm), and hemisphere (depth 6mm and diameter 6 mm). The details in these samples, such as the cone's tip of the hemisphere's bottom were considered comparable to the samples printed (with voids) for the partial discharge experiment.

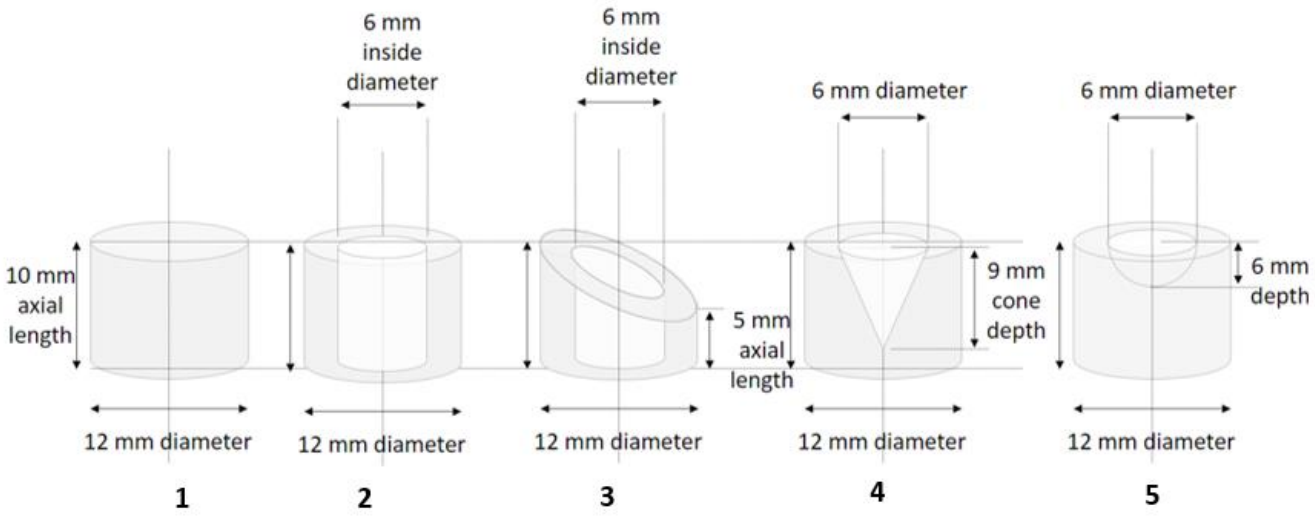

(a)

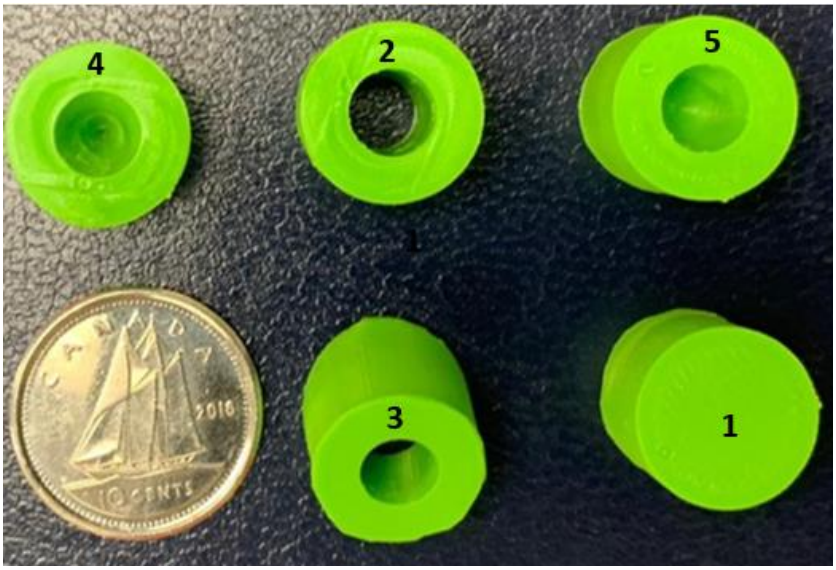

(b)

Figure 3.6: Sample with voids of different shapes (hollow cylinder, slanted hollow cylinder, cone, and hemisphere) at the surface of the sample. (a) Diagram of the design of the samples with void at surface. (b) Image of the 3D printed samples with void at the surface.

The research objective is to use PLA sample to provide a testing environment for fundamental studies of partial discharge generation from voids. Over time insulation materials

develop voids/air gaps from which partial discharge occurs. Samples with voids and control samples (i.e., without voids) were designed and printed, to compare the amount of partial discharge observed for samples with different sizes of voids and benchmark this against the response from the control sample.

The sample with voids were cylindrical with voids located on the axis of rotational symmetry (Figure 3.7). The control sample was a solid cylinder of external dimensions 12 mm (height and diameter). The 3D- printed cylindrical samples had either a single void or multiple voids along the axis of rotational symmetry. The dimensions of the multiple voids (height same as diameter) were 2 mm, 1 mm, 0.75 mm, and 0.50 mm in a sample of overall height 20 mm and diameter 10 mm, while the samples with single voids were printed with individual voids of 12mm (height and diameter). These samples were scanned/imaged using X-ray microtomography to confirm the presence and dimensions of the void (which, for these designs, cannot be viewed non-destructively via any other technique).

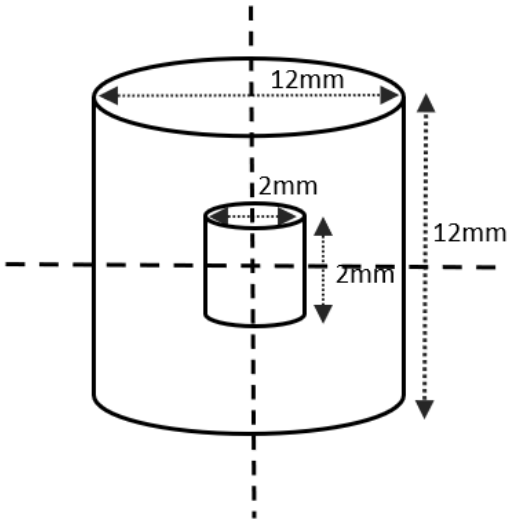

Figure 3.7: Cylindrical sample with external dimensions 12 mm (length and diameter) showing the location of a small cylindrical void at the mid point of the cylindrical axis.

3.2. Physical Characterisation

Physical characterisation of the printed sample involved optical and non optical techniques using optical microscope, profilometry and atomic force microscopy. In addition, the densities of the 3D-printed samples were determined.

3.2.1. Optical Microscopy

An *Olympus BX511TRF* optical microscope was used to observe the surface of poly-lactic acid samples.

Figure 3.8: Olympus BX511TRF optical microscope used to study the sample surface.

The samples observed were cylindrical samples of diameter 12 mm with voids of different shapes of dimensions 0.5 mm (height/diameter/length). The samples had voids at the surface of

different shapes including triangle, square, circle, and ellipse. During this experiment the inner structure of the voids were studied

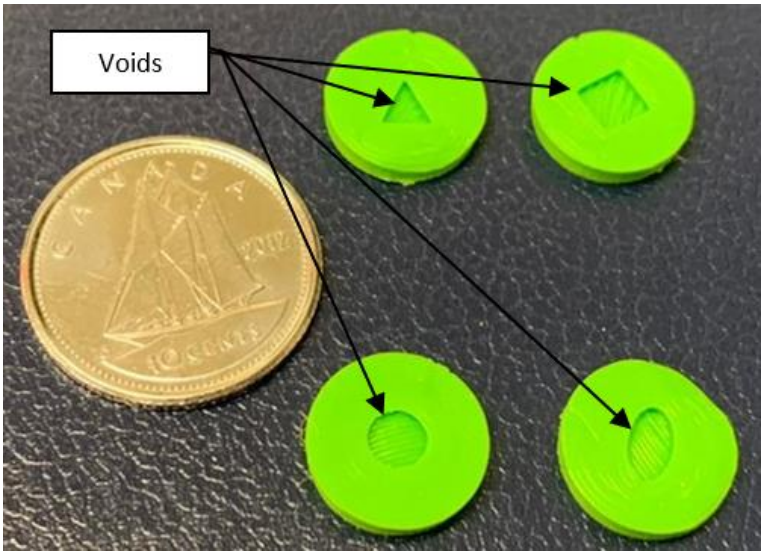

Figure 3.9: Samples with 12 mm (outside) diameter and 0.50 mm (inner height/diameter/length) voids in the shape of triangle, square, circle, and ellipse at the surface.

The print lines on the inner surface and at the bottom surface of the samples were magnified to understand the roughness and imperfections occurred during printing the sample. This method was used first for roughness analysis as optical microscopy is faster and has fewer constraints compared to atomic force microscopy. Furthermore, the depth of the sample was noted to verify the deviation between designed sample and the printed sample. The same samples were later analysed using profilometry and the results of the two were compared.

3.2.2. Atomic Force Microscopy

Atomic Force Microscopy is a technique that provides nanoscale measurements of surface topography. The technique exploits the interaction between a sharp probe (tip) at the end of a cantilever, the entire assembly having been micromachined from silicon. A laser beam is focused on the back of the cantilever, the reflected position of which is detected by a 4-segment split photocell. The spatial variation in the position of this reflected beam provides the raw data from which the surface topography may be reconstructed. As the probe is rastered across the surface of the sample, the photo detector data (variation in laser beam deflection) can be correlated with specific locations, resulting in a representation (image) of the surface topography.

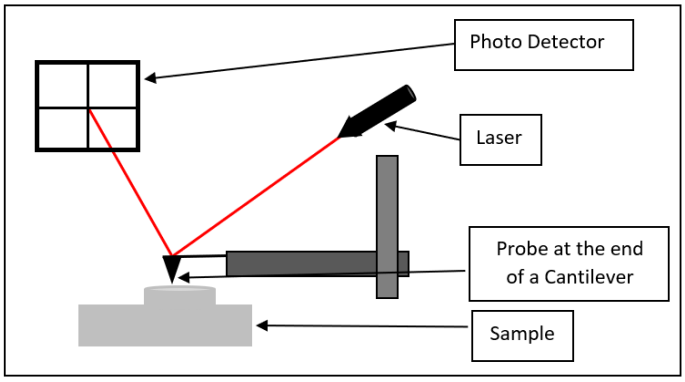

Figure 3.10: Working Principle of Atomic Force Microscopy.

The *Veeco D3100* AFM supported by *Nanoscope* software to obtain images of the sample surface with nm scale resolution [32]. The *Veeco D3100 Atomic Force Microscope* has a piezoelectric tube actuator responsible for the precise positioning of the probe/cantilever while the sample is being scanned. The sample was attached to a specimen disc and placed below the probe assembly. After placing the sample, the laser is adjusted manually using set screws while optimizing the photodetector output. Thus, the laser spot is focused on the cantilever with the

reflection is near the split photodetector's centre. Once the adjustments are made, the stepper motor is engaged bringing the tip close to the sample surface to start scanning using the piezoelectric tube. This AFM has three different modes of operation depending on the material of the sample to be scanned. The first mode is the *contact mode*, wherein the probe tip remains in contact with the surface while tracing the sample. The probe is pushed against the surface, slightly bending the cantilever. Variation in sample topography is detected by variation in how much the cantilever bends, and the instrument controller corrects for these variations, regaining the original position of the spot on the photodetector. The second operational approach, called tapping mode, is the process that sees the probe tip intermittently in contact with the surface. The cantilever/probe is vibrated at the mechanical resonance of the cantilever, and small variations in this resonance are detected due to the interaction of the probe tip and the surface. The last operation mode is magnetic force microscopy, in which magnetic samples are scanned using a magnetized tip (achieved with a cobalt or chromium coating) [32].

The roughness of the scanned area is represented in terms of parameters such as *absolute roughness* (R_a) which is the arithmetic average of the absolute values of the surface height deviation measured from the mean plane, *root mean square roughness* (R_q) which is the average of height deviation taken from the mean image data, and R_{max} which is the maximum vertical distance between the highest and lowest data points in the image following the plane fit [33].

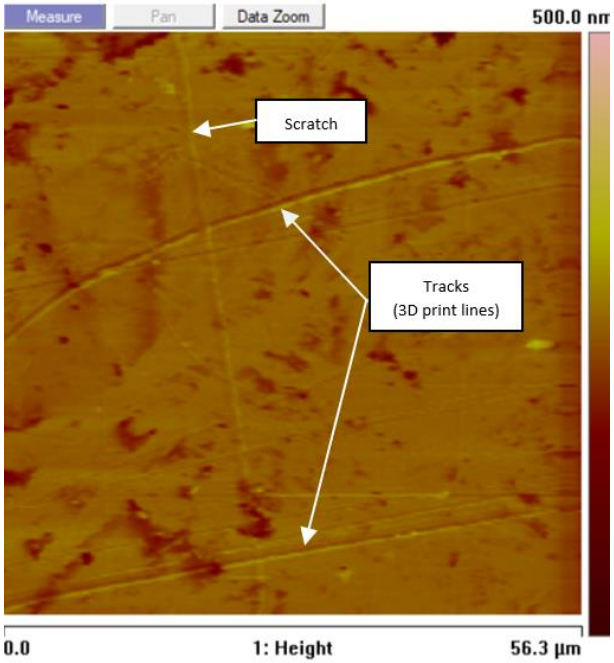

Figure 3.11: AFM Image of area between the tracks (3D print lines) of a cylindrical disc sample with some imperfection and scratches on the disc.

3.2.3. Profilometry

The *KLA- Tencor AlphaStep 500 (AS 500)* profiler is a stylus-based surface profiler that can be used to record single-line traces. Profilometry is a technique to understand the topography of the surface for a given sample that involves a single stylus (or probe) used for a single point or a line scan. Profilometry aimed to quantify print lines' surface roughness and, height before and after "ironing" the PLA sample. A probe is maintained in contact with the sample in the profilometer as it is passed across its surface. The probe follows the surface contour, and its relative "height" is recorded for analysis [34]. The operating ranges of the AS 500 profilometer are a maximum thickness of 10 mm, a maximum single scan length of 300 µm, and a variable image magnification of 10 Ångstrom.

Profilometry was also used to understand the samples (figure 3.8) designed with voids at the surface. The samples used were cylindrical samples of diameter 12 mm with voids of different shapes of dimensions 0.50 mm (height/diameter/length). The samples were scanned by the probe creating a map to analyse the sample's topography.

Profilometry was used to obtain the void's depth (relative to the uppermost surface) and compares the roughness and heights of any traces (print lines) in both locations. Depth measurements were compared to the results obtained from optical microscopy and the desired depth from the original design file.

3.2.4. Density

The mass density of PLA sample is consequence of the fabrication process. A pair of samples with same fabrication process, i.e., printed from the same design file using the same printer settings, were studied for volume and density. To analyse the density, the sample was weighed using a *Perkin Elmer AD 6 Auto Balance* (microbalance) and the volume of the sample was measured using the displacement of water.

Each sample was immersed in a known volume of water contained within a graduated cylindrical flask. The (change) rise in water level due to the fully immersed sample was recorded as the volume of the sample. The sample did not absorb water during this process (confirmed independently).

3.3. Dielectric Spectroscopy

Dielectric spectroscopy is a technique used to determine the dielectric constant (ε'), dielectric loss (ε"), and conductivity (σ') as a function of frequency. The *Solartron Analytical Modulab XM Material Test System* (dielectric spectrometer) was used for the dielectric measurements of the PLA samples. This dielectric spectrometer can measure the dielectric properties of samples over the frequency range from 10 μHz to 1 MHz. The frequency range to be selected and apparatus to measure the dielectric permittivity depend on the samples's nature to be investigated. In the case of high frequency experiments (>MHz), distributed circuits methods are chosen, while at lower frequencies the sample holder forms a parallel plate or a cylindrical capacitor [35].

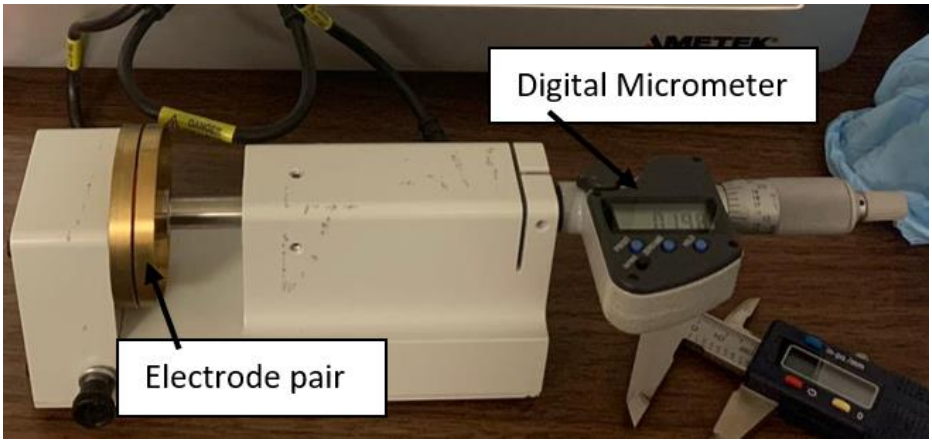

Figure 3.12: An image of the Solartron sample holder with the brass electrodes and digital

micrometer.

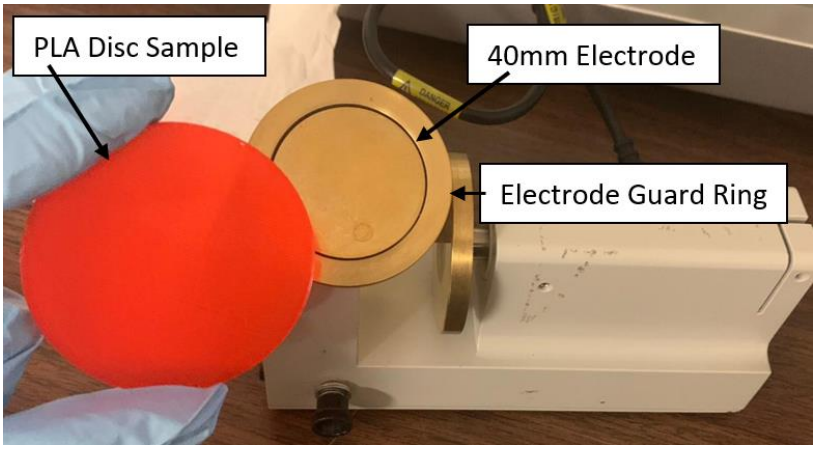

Figure 3.13: An image of the 60 mm PLA Disc sample and 40 mm replaceable electrode with guard ring.

The sample setup for the experiment (Figure 3.12) shows the *Solartron* sample holder with a fixed ground electrode and one movable brass electrode connected to a digital micrometer to record separation between the electrodes. The guard ring around the electrode (Figure 3.12) reduces the effect of the fringing electric field. This sample holder is compatible with various electrodes, which are chosen based on the sample size. The electrodes used for the dielectric measurement of the PLA disc samples had a diameter of 40 mm. The cylindrical discs of PLA had thicknesses ranging from 300 µm to 1000 µm.

The PLA sample was placed between the brass electrodes. The movable electrode used was 40 mm and 55 mm in diameter with the addition of a guard ring, tightened onto the holder with a screw, bringing the overall diameter to 55 mm. The sample holder is connected to the general measurement module supported by *Solartron Modulab MTS* software and dielectric measurements were performed over a frequency range of 1 Hz to 10^5 Hz. The ambient room temperature for all the measurements was 22 °C. The dielectric constant of the sample was

measured using connections to the general measurement module. The thickness of the samples was measured independently using a digital calliper before being placed in the sample holder and later entered into the software.

3.4. X-ray Microtomography

In this technique, x-ray irradiation was used to produce a three-dimensional representation of the sample structure by combining the sample's two-dimensional shadow images (slices). With the sample mounted to a rotating fixture and the x-rays were projected perpendicular to the axis of rotation. As the sample was rotated in the beam, a series of absorption measurements was taken producing a shadow image (as a function of rotation angle). Each point on the shadow image contained the absorption information inside the object corresponding to the x-ray beam at a specific angle to the original sample. Rotating the sample added more data from which a reconstruction of the localised absorption point was obtained using mathematical tomographic reconstruction algorithms, creating a "slice" or planar image of the region of the object in the beam. Three- dimensional images of the overall sample were obtained using software tools to combine a series of reconstructed two-dimensional shadow images.

The micro-tomography (micro-CT) was performed by a *SKYSCAN – 1275* [36] instrument consisting of a (micro-CT) scanner, and a computer system with control, reconstruction, and application software. The image slices were sequentially processed through multiple software tools to obtain the three-dimensional reconstruction of the object. The instrument is supported by the software *Skyscan1275,* which controls the instrument and runs the x-ray beams. *NRECON* software removed the noise during the post-processing and constructed the 2D images. Reconstruction of the two-dimensional shadow images to three-dimensional image was achieved

using the software *CTVOX*. Finally, the three-dimensional scan was analysed by adjusting the transfer function of the scanned object using *CTAN* software [36].

When placing the sample for scanning - the sample was fixed to a removable sample holder that, in turn attaches to the rotating stage of the instrument *SKYSCAN-1275* [36]. Dental wax was used at each attachment point enabling the easy removal of the sample after scanning.

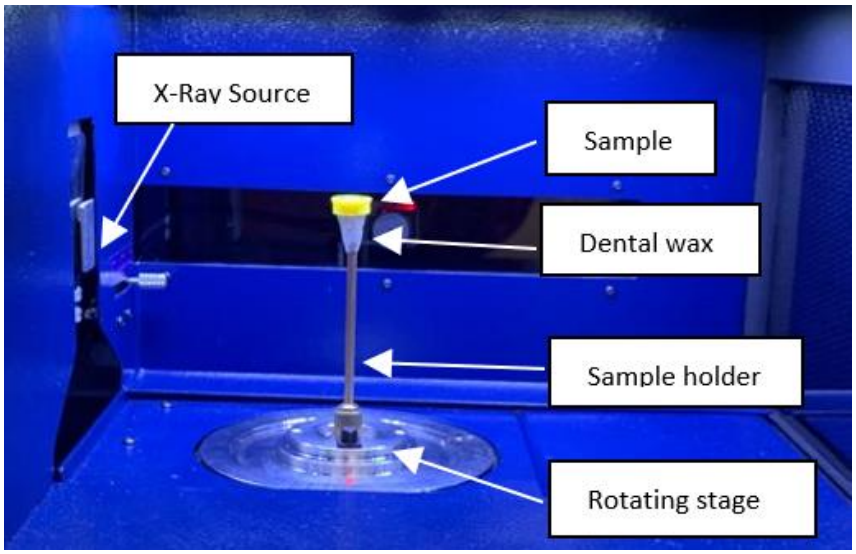

Figure 3.14: Sample window of SKYSCAN-1275 with sample on the removable sample holder supported by dental wax and sample holder attached to the rotating stage of the instrument.

Before running the scans, the instrument *SKYSCAN-1275* was switched on, and the x-ray generator was allowed to reach steady state. The time to reach this state depends on the voltage used and the choice of x-ray beam filter. The voltage is determined by the density of the sample material. For a voltage between 40 V and 60 V no filter is selected, for 60 V to 80 V an aluminium filter is used and, for voltages over 80 V, a copper filter is used. For these samples, the voltage selected was 40 V at a current of 250 µA (i.e., no filter was used). The samples designed for this study were sufficiently small that the source could remain in close proximity to the sample, optimizing the instrument resolution.

When operating, the control software shows a real time image through the camera in the sample window (Figure 3.14). The sample's rotation rate (degree step) during the scan was selected to be 0.2°. After choosing the settings, the sample was scanned, each scan took approximately fifteen minutes giving the two-dimensional shadow images.

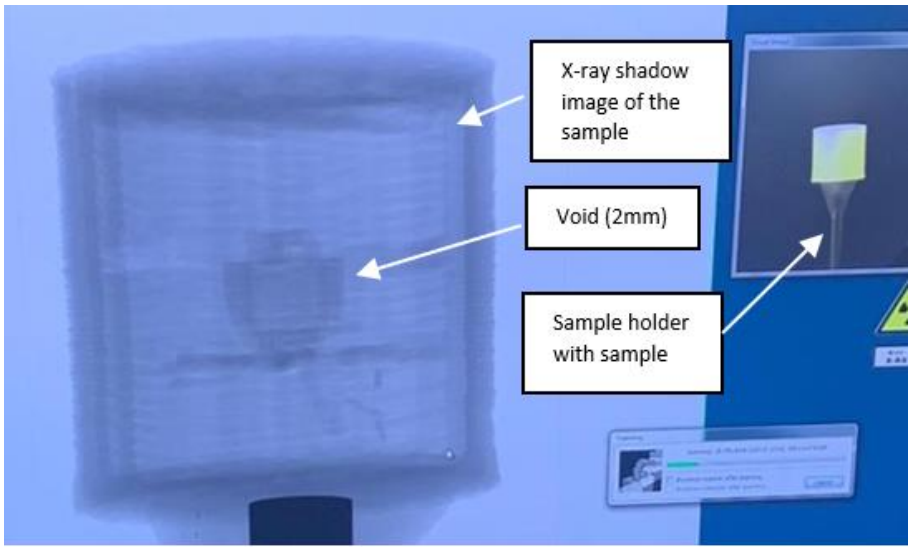

Figure 3.15: X-ray shadow image of sample with single void (height 2 mm and diameter 2 mm) alongside the camera image of sample being scanned.

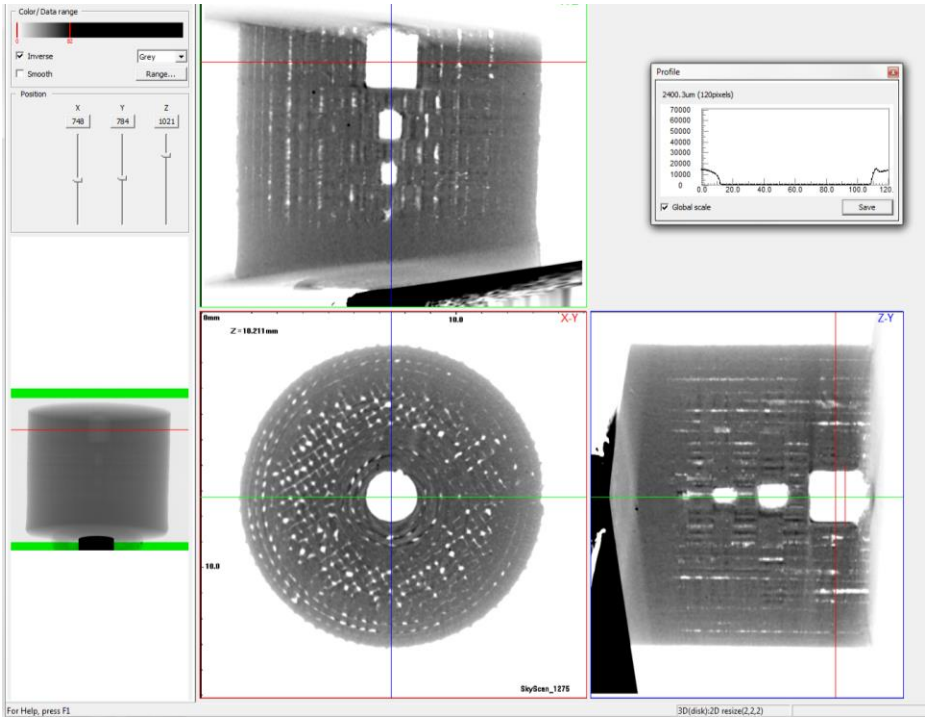

Figure 3.16: Two-Dimensional view of the sample with multiple voids along the red line seen in the left image. The three images are along the axis X-Z (top), X-Y (Bottom left) and Z-Y (Bottom right).

All samples were scanned in order to understand the fabrication process and limitations, the overall goal was to create a sample with smallest amount of imperfection that would distract from the partial discharge signature associated with the void. Multiple samples were analysed with several combination of printer setting, and design alteration. These settings are documented completely in Appendix B.

3.5. Partial Discharge Measurements

Partial discharges in dielectric material occurs due to the presence of void or an air-filled cavity. A partial discharge is the event in which a discharge starts from one end of the void, bridging through the air gap and reaches the other end of the surface. Thus, partial discharges do

not bridge the insulation between electrodes but just the cavity in the insulation. As the permittivity of air is less than the permittivity of the PLA material surrounding the void, the electric field in the void is higher than in the surrounding material. Once the electric field in the void is high enough, breakdown strength is exceeded creating a partial discharge.

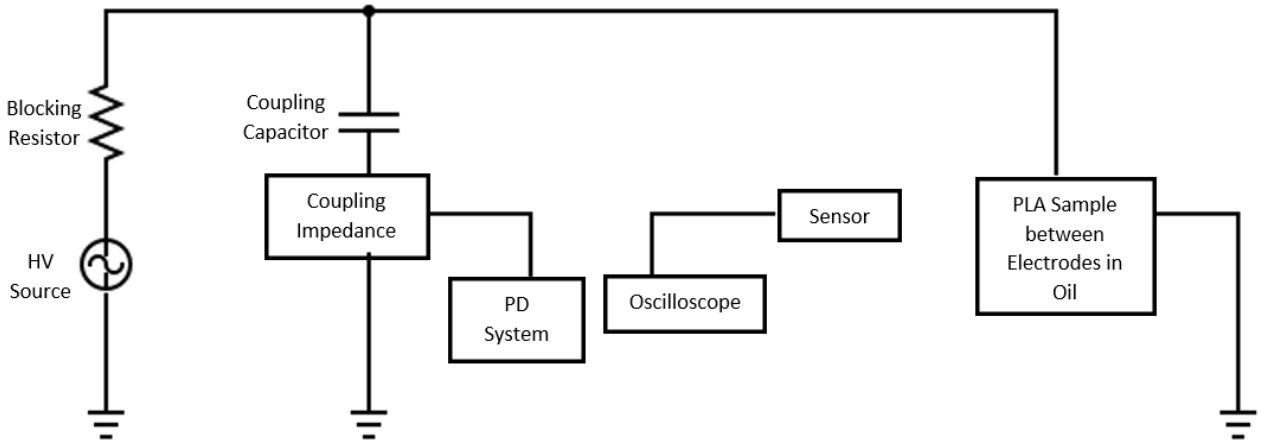

Figure 3 17: Experimental setup for the partial discharge measurements with multiple components including a high voltage source, coupling capacitor, and coupling impedance, partial discharge system (Omicron MPD600), a 2.5GHz digital oscilloscope and sample in the sample holder.

Figure 3.18: Experiment setup for partial discharge measurements in laboratory

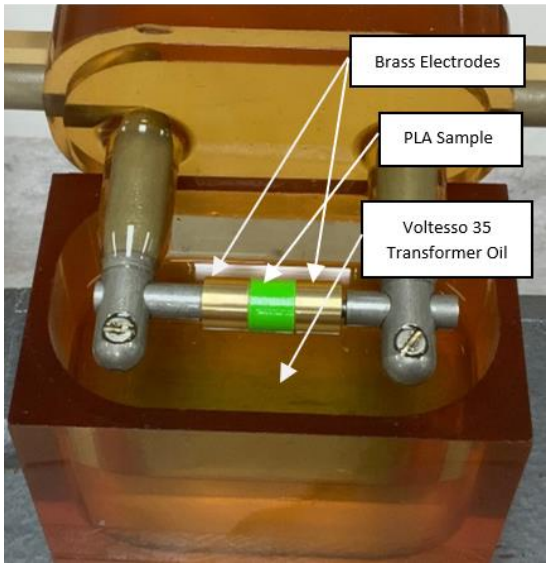

Figure 3.19: Sample holder with two brass electrodes of (10 mm diameter) on both side of the PLA sample (12 mm diameter) to be immersed in Voltesso 35 transformer oil during the partial discharge experiment.

The partial discharge measurements for each sample were taken after completing the microtomography and determining the shape and size of the voids. The samples were placed in a chamber between two brass electrodes of 10 mm diameter immersed in transformer oil *Voltesso 35* and connected to the partial discharge setup (Figure 3.19). To determine if absorbed oil in PLA sample affect discharge, some samples were immersed in oil for two weeks. These were weighed before and after immersion, and the discharge measurements compared with samples, that were never put in oil. The mass measurements of these samples were obtained using a *Perkin Elmer - AD 6 Auto Balance*. The mass variations recorded were within due to instrumental uncertainties, confirming that the PLA samples did not absorb oil (which would interfere in the partial discharge measurements).

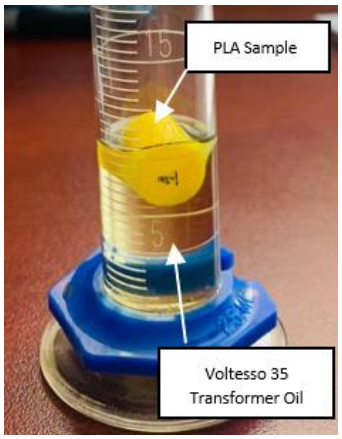

Figure 3.20: Image of a sample immersed in Voltesso 35 transformer oil.

Once the electrode and the sample were immersed in transformer oil, the connections were made to the *Omicron MPD600* and the *Variac* were used to adjust the voltage. Each 0.1V voltage step of the *Variac* corresponded to an increase of 36.7 V in the voltage across the sample. Phase resolved partial discharge pattern (PRPD) were determined by the *Omicron* software. For some samples the partial discharge was accompanied by sparks and a buzzing sound. The voltage at which partial discharge starts in a sample is known as the partial discharge inception voltage (PDIV), after inception the voltage was increased further for few seconds to check for increase in strength and magnitude after which the voltage is gradually reduced till the voltage at which partial discharge completely disappears which is called partial discharge extinction voltage (PDEV). The phase resolved partial discharge patterns were recorded, studied and analysed.

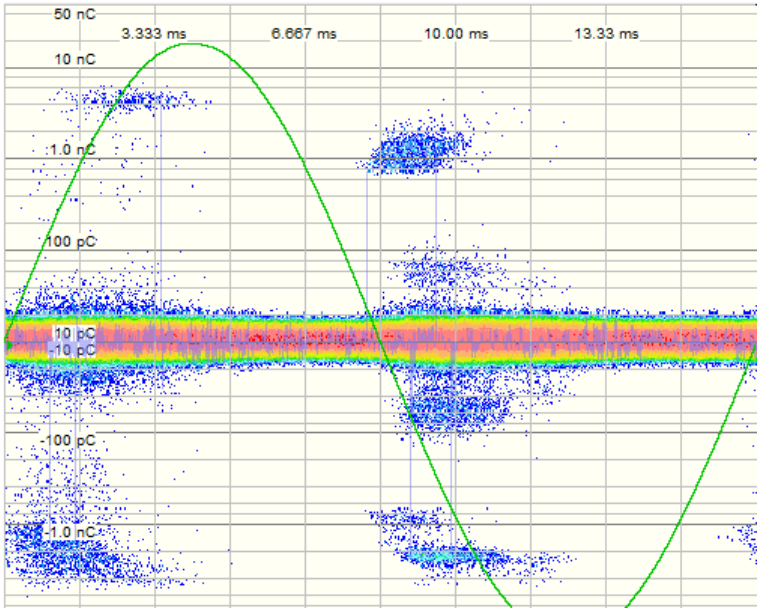

Figure 3.21: Example of a PRPD pattern obtained from a PLA sample (12 mm height and diameter) with a 0.75 mm void at the center of the rotational symmetry axis. This sample had an inception voltage 13.33 kV

The samples under testing had same diameter but different heights. The smallest sample was 5 mm in height and the largest sample with height 12 mm, along with sample the void size varies from 2 mm to 0.50 mm. The experiment aims to understand the dependency of the size of void and the voltage at which partial discharge would occur due to that void.

Chapter 4

Results and Discussion

4.1 Summary of Physical Characterisation

The analysis and results obtained from optical and non-optical techniques to understand the surface of the sample, the inner structure of the voids and the precision of the manufacturing process.

4.1.1 Mass and Density

The density experiment confirmed that though there was a difference in the weight of the samples, but the (mass) to volume ratio (mass density) of the samples were same. In essence, the variations in mass could be attributed to a lack of precision in the fabrication process resulting in slight differences in sample size, rather than sample density.

4.1.2 Results of Atomic Force Microscopy

The samples analysed by atomic force microscopy were PLA discs. Roughness measurements (Table 4.1) for the area between the tracks (print lines), on the tracks, in-line of the tracks (dotted line in Figure 4.1 illustrates the movement of the probe) and the side towards the print bed (reverse side) for both non-ironed and ironed sample.

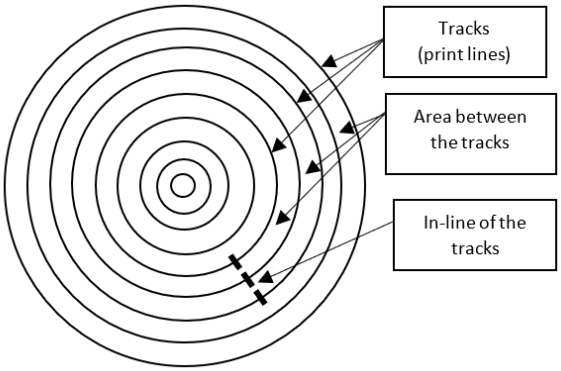

Figure 4.1: Representation of the PLA disc sample printed using fill pattern setting as concentric circles displaying the track (print lines), area between the tracks and a doted line showing the movement of probe in-line of the tracks.

Table 4.1: Absolute roughness, root mean square and maximum vertical roughness value in nanometer for non-ironed and ironed sample.

	Non-ironed samples			**Ironed samples**		
	R_a (nm)	R_q (nm)	R_{max}(nm)	R_a (nm)	R_q (nm)	R_{max}(nm)
Area between the track	12.2	17.9	300	3.22	4.55	138
On the track	49.4	57.8	261	379	821	7957
In a line with the track	152	274	1861	212	607	8246
Reverse side	116	448	3480	475	605	4862

Atomic force microscopy confirmed that the ironing technique made the surface between the tracks smoother but increased the roughness on individual tracks. Ironing on the reverse side (side towards the heated printer bed) increased the roughness of this side.

4.2 Summary of Dielectric Spectroscopy

Dielectric spectroscopy was performed to document the dielectric properties of PLA samples. The experiment was to determine the dielectric constant of the PLA disc sample of different thickness.

Table 4.2. Dielectric constant of PLA cylindrical disc samples of different thickness measured by dielectric spectroscopy at the average of frequency range of 1 Hz to 10^5 Hz.

Designed Thickness	**Sample**	**Measured Thickness**	$\|\varepsilon_r\|$
300µm	A	300	1.99
	B	286	1.93
	C	300	2.35
	D	316	2.49
500 µm	A	500	1.70
	B	521	2.20
	C	502	1.98
	D	543	2.60
1000 µm	A	1000	2.04
	B	1118	2.31
	C	1079	2.50
	D	999	2.67

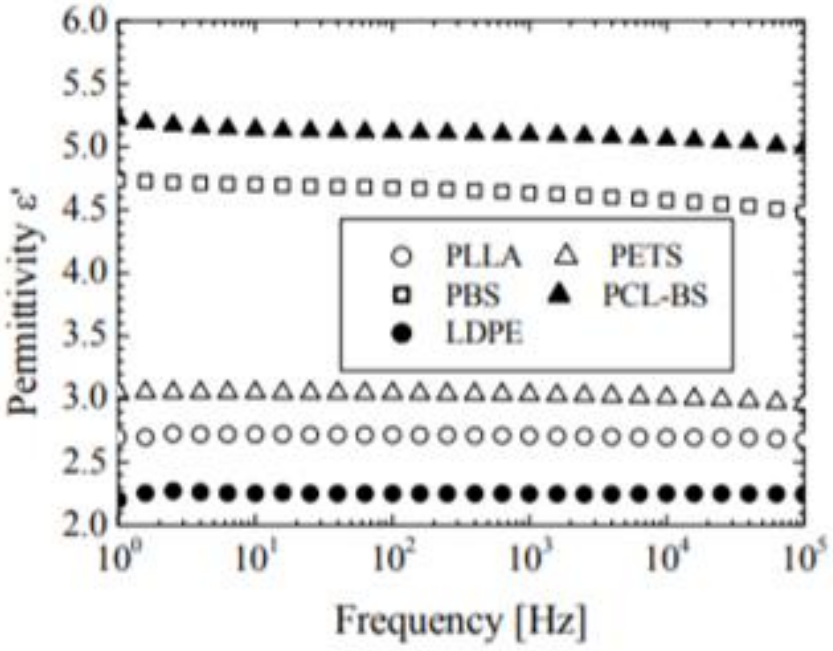

Figure 4.2. Permittivity values of PLLA (poly-L-lactic acid) and other polymers as a function of frequency. The expected value of permittivity of PLA is 2.7 which is comparable to 2.38 for a 1000 µm thick PLA disc sample *(Figure 3 from [37], © 2007 IEEE)]*

The results obtained from dielectric spectroscopy are comparable to the literature. The deviation and inconsistency in the results is due to the imperfections and visible gaps between the print lines on the uppermost surface of the sample. Finite element simulation using *COMSOL Multiphysics* software (Appendix A) was used to confirm this assertion. The simulations incorporated comparably scaled imperfections at the sample's surface and show a response in the measured relative permittivity that is consistent with the data in Table 4.2.

4.3 Results from x-ray Microtomography

Microtomography scans were performed on the samples to understand the fabrication of the sample and confirm the presence and placement of the void in the sample. This is the best technique to get an understanding of any inner structure within the control samples as well as the precise dimensions of voids in that remainder of the samples.

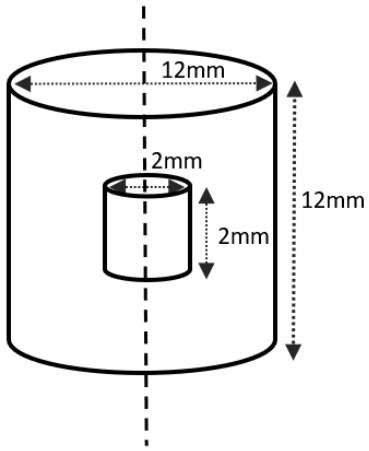

Figure 4.3: Cylindrical sample with dimensions 12 mm (height and diamter) with a 2 mm (height and diamter) void at the centre of the sample.

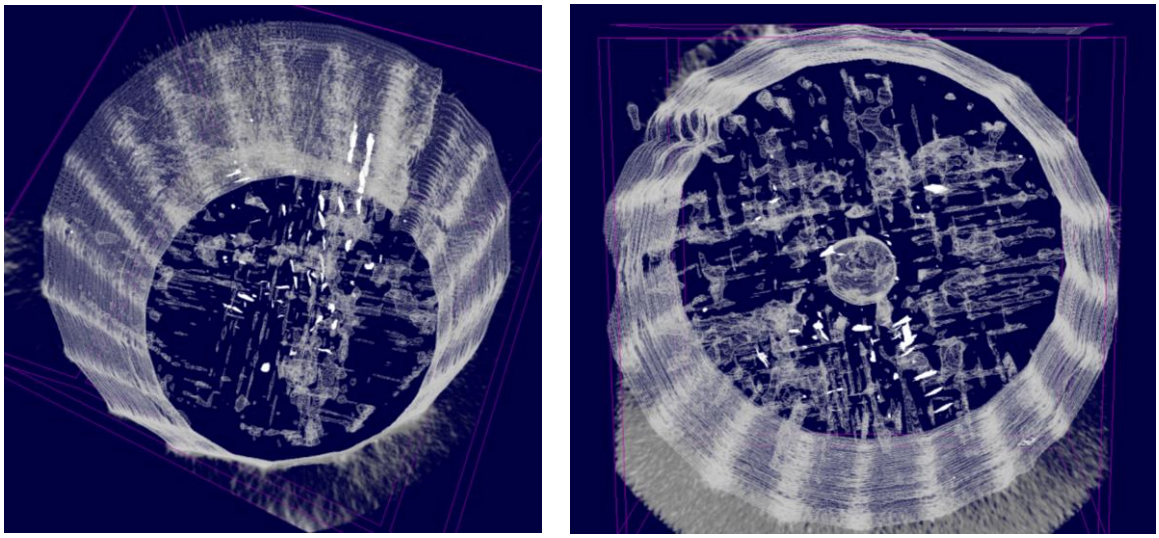

(a) (b)

Figure 4.4. (a) Three dimensional top view of control sample with imperfections. (b) Three dimensional top view x-ray scan of sample (Figure 4.3) with a 2 mm (height and diameter) void at the centerof the sample.

Microtomography scans confirmed the presence of voids along the rotational axis of the cylindrical sample. Additionally, it helped in understanding fabrication process better. Figure 4.4(b) and Figure 4.5 show examples of samples with numerous imperfections in the solid area of the sample along with voids. The occurance of imperfections in the solid area along the print lines and the distortion in the shape of the void suggested the need for a change in the printer setting and sample design to reduce the number of imperfections within the sample. In order to get a sample with fewer imperfections, the infill patterns was changed from concentric to rectilinear and ultimately, to aligned rectilinear. As part of this optimization process, samples were printed at different flow rates: 90%, 92%, 95%, 98% and 100% (representative images and data sets in Appendix B). These were later all scanned using x-ray microtomography to document the effect of flow rate on the samples (control and with void).

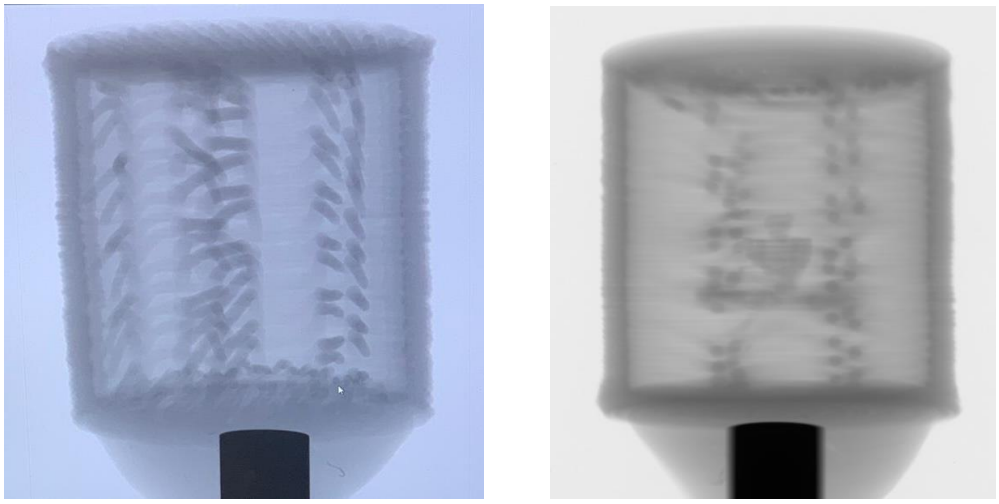

(a) *(b)*

Figure 4.5. X-ray shadow image of a control sample and a sample with void including imperfections created during printing. (a) X-ray shadow image of control sample with imperfections along the print lines. (b) X-ray shadow image of sample with a void of 1mm (height and diamter) along with imperfections around the void.

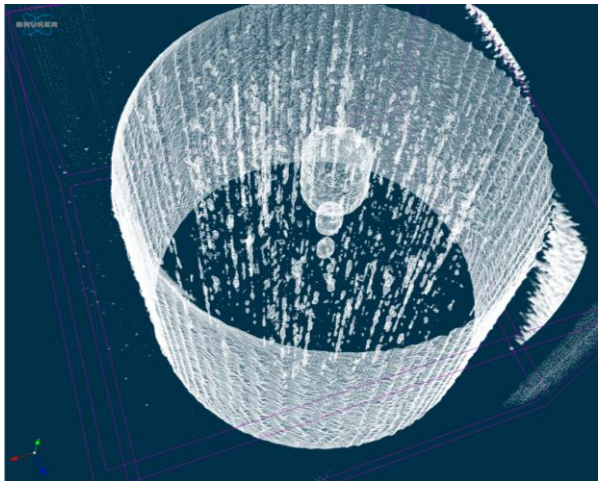

Figure 4.6: Reconstructed 3D top view of the sample with multiple voids (in Figure 3.13) Showing voids along the axis of the sample and imperfections in the solid sample surface.

The printer settings that were tweaked in order to get better samples were flow rate, nozzle temperature, printer bed temperature, ironing and infill. The flow rate that best suited for the

sample was 100% - this reduced the number of imperfections present in the solid area of the sample. When the flow rate was increased, it was observed that the voids smaller than 0.75 mm were either filled by PLA material or had a distorted shape. Therefore, samples were made with voids of 1 mm and 2 mm in order to focus on characterizing voids that reflected their design (printing) dimensions and providing a basis for future refinement. The printer nozzle temperature selected was 220 °C to control the amount of extrusion from the nozzle to significantly reduce imperfections and get voids of the same dimension as designed. The printer bed temperature best -suited for these samples was found to be in the range 75 °C – 85 °C. It was observed that the layers closer to printer bed had fewer imperfections.

After analyzing multiple samples with voids of different dimensions alterations were done in the sample design and multiple combination of printer setting to create a sample with least imperfection (see Figures 4.7 and 4.8).

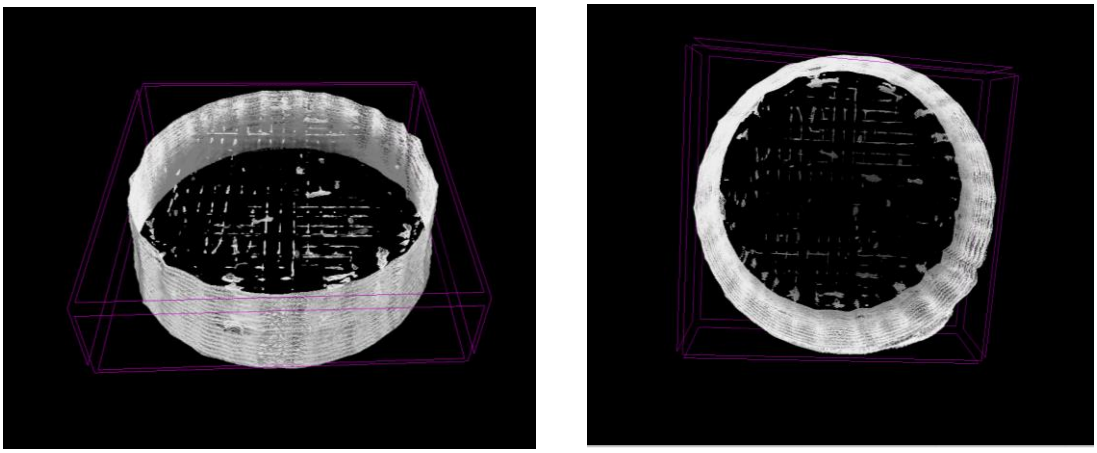

(a) (b)

Figure 4.7: Reconstructed three dimensional image of a control sample with 5 mm height and 12 mm diameter (a) Top view of the sample showing imperfections at the surface. (b) Bottom View of the sample showing imperfections only in the upper layers of the sample.

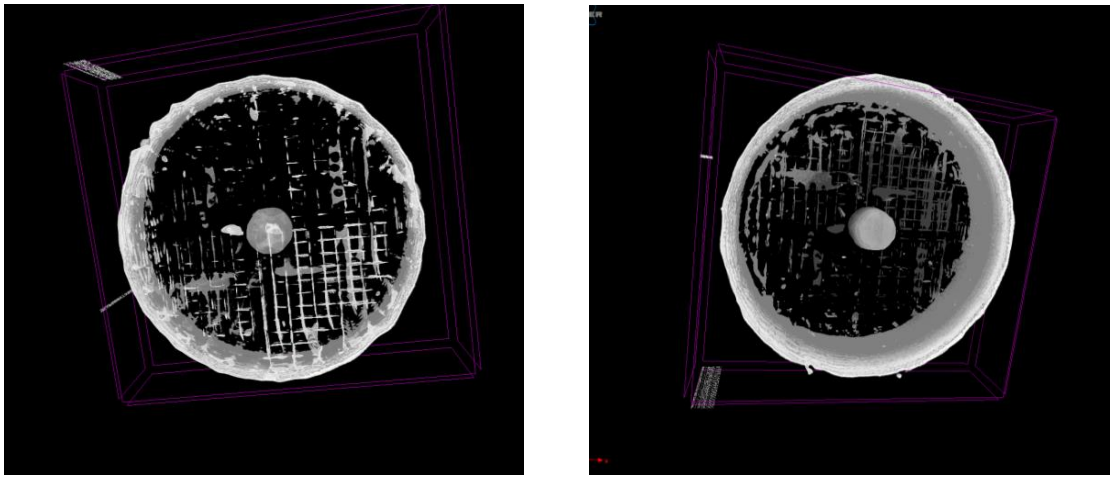

(a) (b)

Figure 4.8: Reconstructed 3D image of sample 5 mm (height and diameter) sample with single void 2 mm (height and diamter) (a) Top view of the sample showing imperfections and void at the center along the rotational axis of the cylindrical sample. (b) Bottom view of the sample showing imperfections only in the upper layers of the sample and void at the center.

The top view of the samples shows noticeably reduced imperfections compared to the samples fabricated before, the layers of the sample towards the printer bed had no imperfection in the solid area.

4.4 Partial Discharge

The partial discharge experiment was performed on multiple samples control samples and samples with voids of different dimensions (single void and multiple voids) as documented in Appendix C. A 60 Hz voltage was applied to the high voltage electrodes with sample in the middle immersed in the transformer oil to stop any surface discharge. The experiment setup was designed according to the IEC 60270 standard [17].

In analyzing the microtomography images it was observed that imperfections occur in the samples during the fabrication process for both control and samples with voids. Further, it is known

that partial discharge occurs by bridging the void (air-filled cavity) in the insulation. The voids designed in the samples help with a better understanding of the voltage at which partial discharge occurs depending on the size of the void.

Partial discharge experiments were performed on a number of samples (comprehensive documentation may be found in Appendix C). Representative experimental data from a control sample, a sample with 2 mm void and a sample with 1 mm void are presented in Table 4.3 followed by the phase resolved partial discharge patterns of these samples.

Table 4.3. Results of PD experiment for control samples and sample with 2 mm, 1 mm and multiple voids of different dimensions.

	Samples (mm)		**Void (mm)**		**Key Voltages (kV)**		
Figure(s)	Height	Diameter	Height	Diameter	PDIV	PDEV	Maximum
4.4(a)	12	12	No void & some imperfections		No PD observed up to 15kV		
4.5 (a)	12	12	No Void		5.33	4.70	6.58
4.4(b),4.9(i)	12	12	2	2	14	-	-
4.5(b),4.9(ii)	12	12	1	1	3.80	3.50	4.40
4.7, 4.9(iv)	5	12	No void & a few imperfections in upper layer		12	12	14
4.8,4.9(iii)	5	12	2	2	12.50	8.20	15
-	20	12	multiple void sample: 2mm, 1mm 0.75mm & 0.50mm		19.64	20.58	23

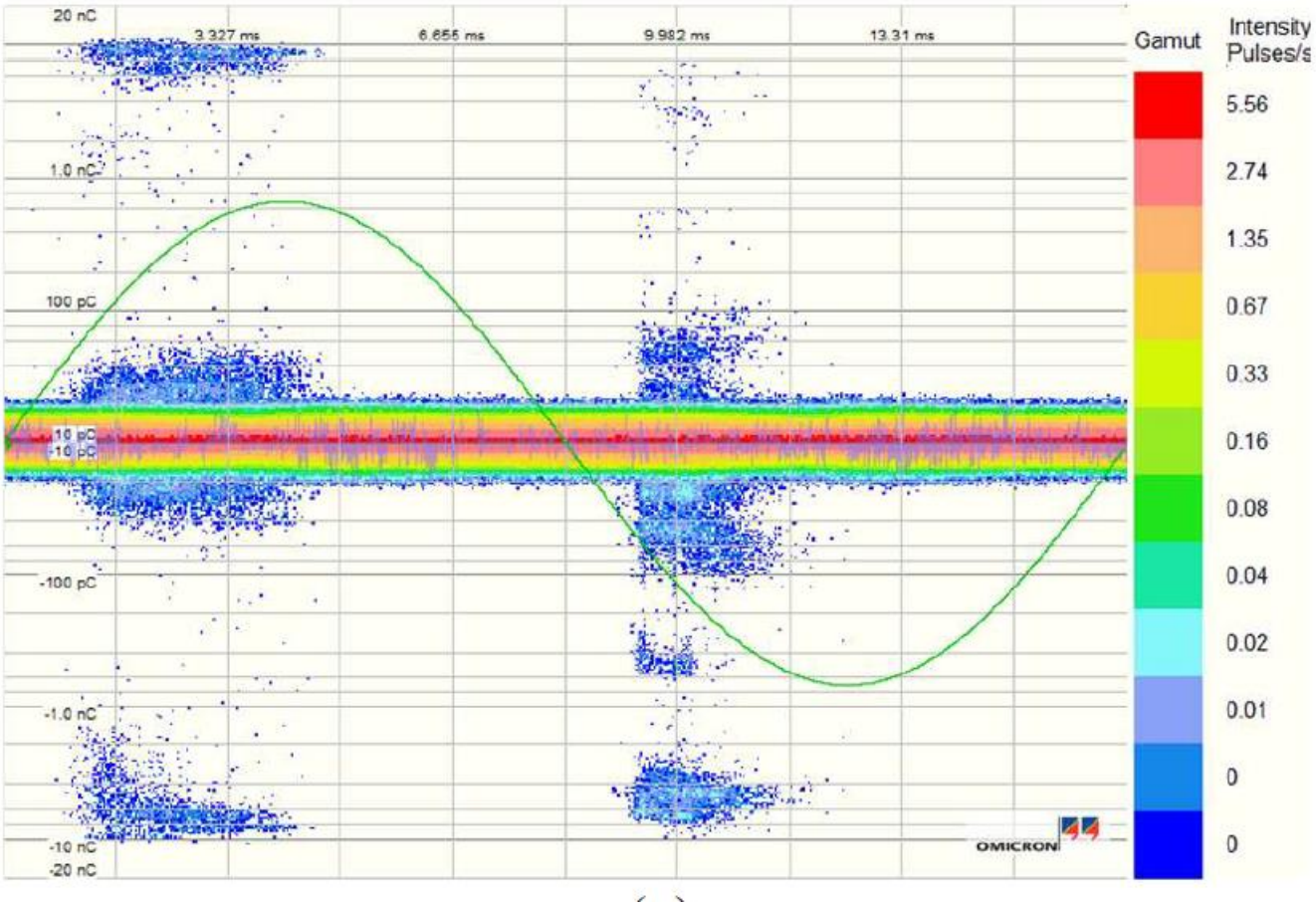

Figure 4. 9. Phase resolved partial discharge patterns for different samples (PD results in Table 4.3.) (i) PRPD pattern of sample of dimensions 12 mm (height and diameter) with 2 mm void at the center of the sample

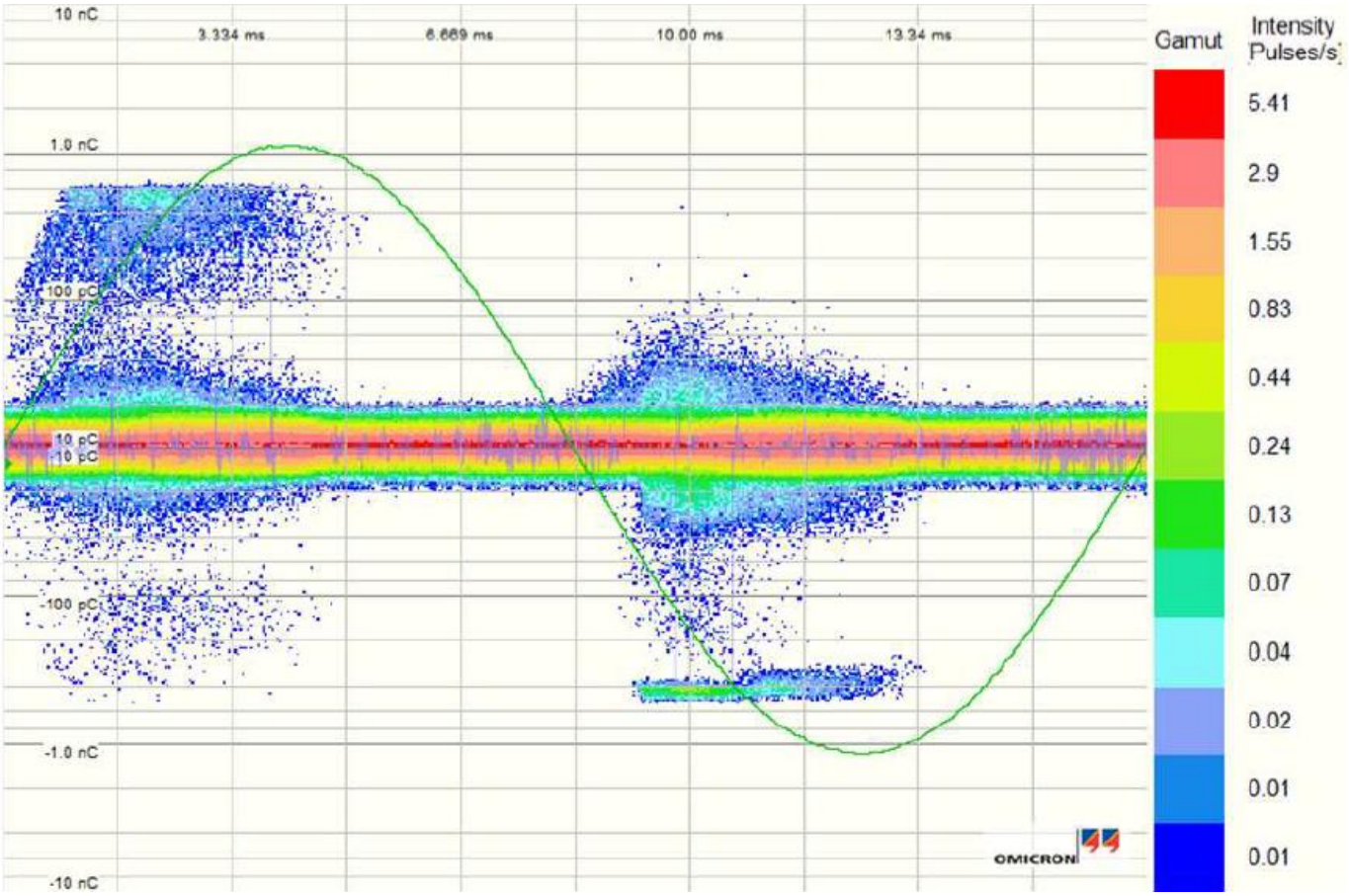

Figure 4. 9. Phase resolved partial discharge patterns for different samples (PD results in Table 4.3.) (ii) PRPD pattern of sample of dimensions 12 mm (height and diameter) with 1 mm void and imperfections around the sample.

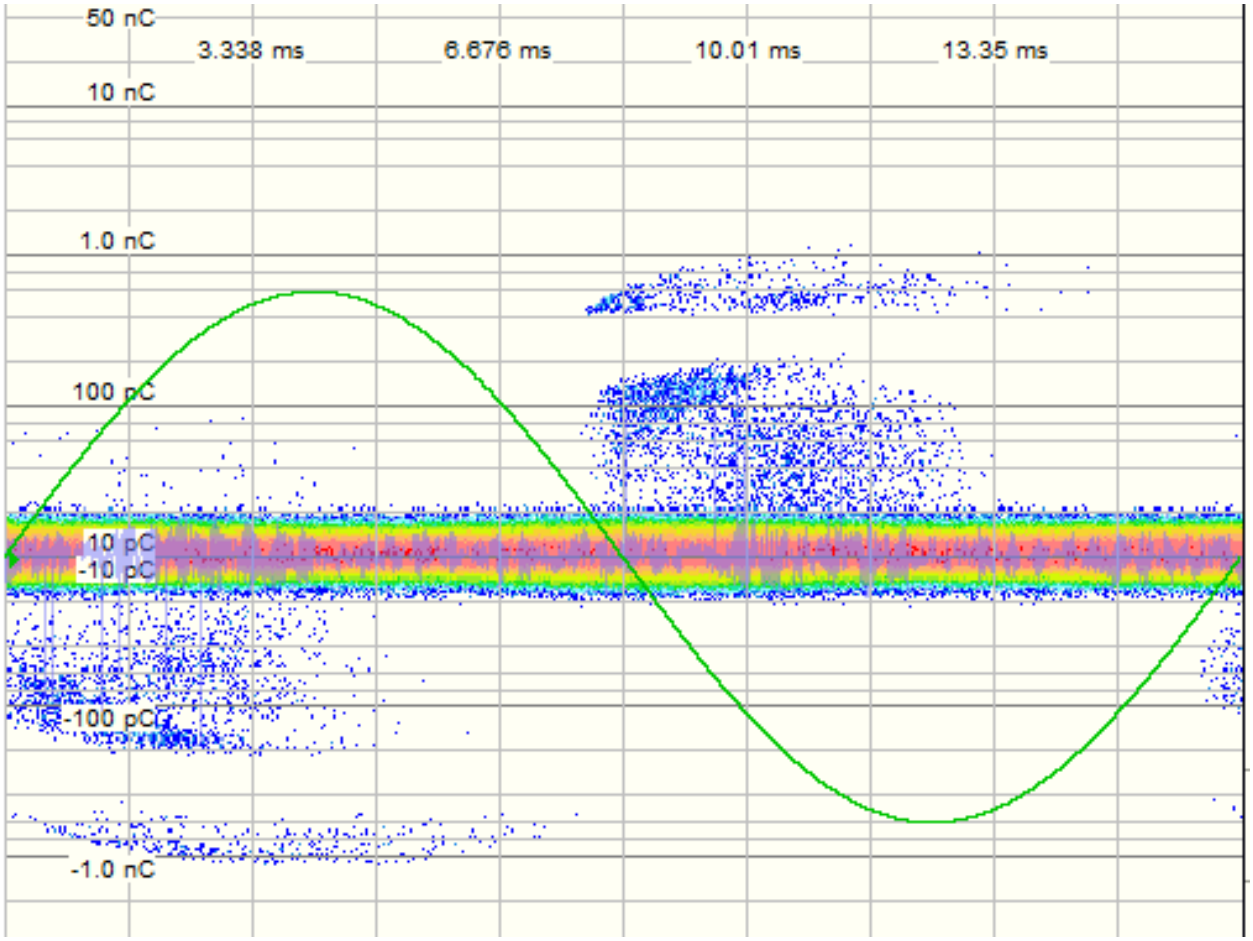

Figure 4. 9. Phase resolved partial discharge patterns for different samples (PD results in Table 4.3.) (iii) PRPD pattern of sample with height 5mm, and diameter 12 mm with 2 mm void at the center of the sample

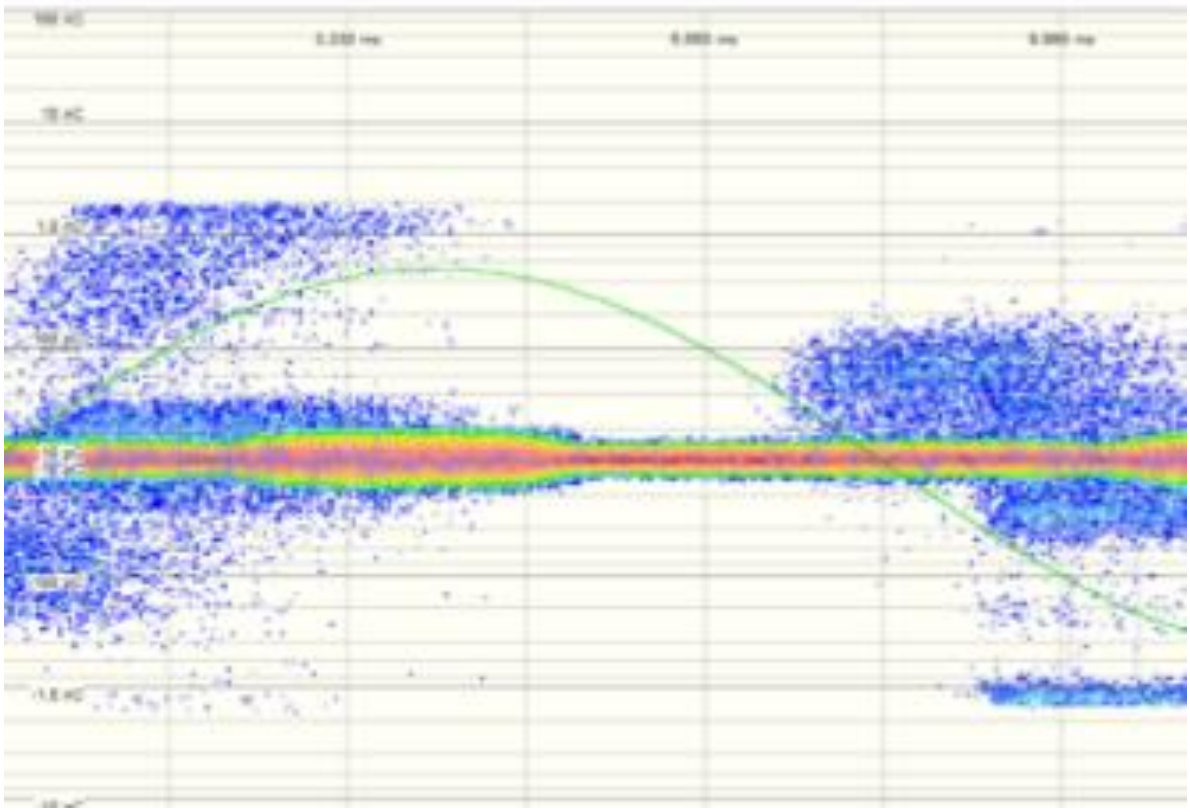

(iv)

Figure 4. 9. Phase resolved partial discharge patterns for different samples (PD results in Table 4.3. (iv) PRPD of a control sample (height 5 mm and diameter 12 mm) with imperfections mostly prevalent in the region of the sample farthest from the heated printer bed.

Some samples with the same dimensions and size of void were found to have different partial discharge voltages. For instance, two control samples with the same dimensions 12 mm (height and diameter) had different results – one did not show any PD voltage till 15 kV and the second has a partial discharge inception voltage at 5.33 kV. X-ray microtomography confirmed the presence and number of imperfections present in the solid area of the sample. The analysis of the results from microtomography and partial discharge indicated that the inception voltage depended on the size of the void in the sample and the number of imperfections in the samples.

For similar samples, those with a larger number of imperfections were found to have lower inception voltages. This can be noted in Figure 4.4(a) and 4.5(a) showing control sample of same dimensions (12 mm height and diameter). The sample shown in Figure. 4.5(a) the later has more imperfections compared to that shown in Figure 4.4(a) and the PD inception voltages, respectively, for the two samples are 5.33 kV and 15 kV. As expected, it was noted that larger samples required larger voltages before PD were recorded.

The PRPD patterns obtained during the experiment were further analysed by collaborators using a convolutional neural network (CNN) attention-based model. The 1D-CNN classification has an accuracy of 98.7%. Adding an interpretable attention model to the CNN shows that the neural networks focus on the regions of the waveform corresponding to the rise of pulse while deciding [38].

Chapter 5

Conclusion

This thesis gives an overview of how PLA can be used as a template system for partial discharge studies. The thesis covers the dielectric properties of PLA and focuses on the additive manufacturing of PLA samples. In particular, methods for creating voids in the samples and documenting these using x-ray microtomography scans of the 3D-printed PLA samples are presented.

5.1 Main Findings

- After printing multiple samples with voids and analysing under X-ray microtomography the smallest void with least distortion in shape was a 2 mm void in sample.
- A combination of printer and slicer settings have been drawn to be able to print a sample with minimum imperfections.
- Voltage at which patrial discharge occurs in the sample is a function of the fabrication process of the sample. We were able to achieve no partial discharge signals for control sample and strong partial discharge for samples with voids.
- It was confirmed that PLA doesn't absorb the *Voltesso 35* transformer oil which was required in order to perform experiments.

5.2 Future Work

With the analysis and better understanding of the additive manufacturing process and the partial discharge behaviour of the PLA samples, it is recommended that the research can be extended in following direction:

- Developing an ideal sample with smaller voids and refine the printer/slicer settings for minimum imperfections in the sample.
- Conduct partial discharge experiment on improved samples and confirm the dependency between partial discharge signals and sample fabrication process.
- Investigate the effect of immersion on PLA sample in transformer oil for a longer time.

References

[1] Omori, Shingo, *et al.* "*Effect of Crystallinity on Electrical Conduction Characteristics of poly (L-Lactic Acid).* " *Japanese Journal of Applied Physics*, Part 1: Regular Papers and Short Notes and Review Papers, vol. 46, no. 6 A, 2007, pp. 3501–03.

[2] Hirai, N., *et al.* "*Dielectric Properties of Biodegradable Polylactic Acid and Starch Ester.* " Proceedings of the 2004 *IEEE International Conference on Solid Dielectrics*, 2004. ICSD 2004, vol. 1, IEEE, 2004, pp. 87–89 Vol.1.

[3] Shinyama, K., and S. Fujita. "*Study on the Electrical Properties of a Biodegradable Plastic.*" Proceedings of the 7th International Conference on Properties and Applications of Dielectric Materials (Cat. No.03CH37417), vol. 2, *IEEE*, 2003, pp. 707–710 vol.2

[4] Teyssedre, Gilbert, and Christian Laurent. "*Advances in High-Field Insulating Polymeric Materials over the Past 50 Years.* " IEEE Electrical Insulation Magazine, vol. 29, no. 5, *IEEE*, 2013, pp. 26–36.

[5] Su, Jingang, *et al.* "*Electrical Tree Degradation in High-Voltage Cable Insulation: Progress and Challenges.* " High Voltage, vol. 5, no. 4, The Institution of Engineering and Technology, 2020, pp. 353–64.

[6] C. Zuidema, W. Kegerise, R. Fleming, M. Welker and S. Boggs, "*A short history of rubber cables,"* in *IEEE* Electrical Insulation Magazine, vol. 27, no. 4, pp. 45-50, July-August 2011.

[7] Liu, Jun, et al. "*Current Advances and Future Perspectives of 3D Printing Natural-Derived Biopolymers.* " Carbohydrate Polymers, vol. 207, Elsevier Ltd, 2019, pp. 297–316.

[8] K. Mathes, "*A brief history of development in electrical insulation*, " in Proceedings of the 20th Electrical Electronics Insulation Conference, Oct 1991, pp.147-150.

[9] Krawczak, P. "*Additive Manufacturing of Plastic and Polymer Composite Parts: Promises and Challenges of 3D-Printing*. " Express Polymer Letters, vol. 9, no. 11, BME-PT Hungary, 2015, pp. 959–959.

[10] T. Nakiri, Y. Kawachi, M. Honda, K. Imoto, T. Yamakita and Y. Tajitsu, "*Development of Electric Wire Using Biodegradable Polymer*," in *IEEE* Transactions on Industry Applications, vol. 43, no. 4, pp. 1069-1074.

[11] R. Arora, and M. Wolfgang, "*High Voltage and Electrical Insulation Engineering*" 1st ed., vol. 57, Wiley, 2011.

[12] Tirado-Garcia, I., *et al.* "*Conductive 3D Printed PLA Composites: On the Interplay of Mechanical, Electrical and Thermal Behaviours.* " Composite Structures, vol. 265, Elsevier Ltd, 2021, p. 113744.

[13] Tofail, Syed A, *et al.* "*Additive Manufacturing: Scientific and Technological Challenges, Market Uptake and Opportunities.* " Materials Today (Kidlington, England), vol. 21, no. 1, Elsevier Ltd, 2018, pp. 22–37.

[14] Blunt, Warren, et al. "*Bioreactor Operating Strategies for Improved Polyhydroxyalkanoate (PHA) Productivity*. " Polymers, vol. 10, no. 11, MDPI, 2018, p. 1197.

[15] Chen, H. C. "*Fractal Features-Based Pattern Recognition of Partial Discharge in XLPE Power Cables Using Extension Method*. " IET Generation, Transmission & Distribution, vol. 6, no. 11, Institution of Engineering and Technology, 2012, pp. 1096–103.

[16] Arora, R., and Mosch, W.., *"7.2.2 "Surface Discharge (Tracking) in High Voltage and Electrical Insulation Engineering.*" *IEEE* Press, 2011.

[17] IEC 60270 (EN 60270) "*High voltage test techniques – partial discharge measurements*" (International Electrotechnical Commission, 2001- amended 2015)

[18] Mohamed, F. P., *et al.* "*The Use of Power Frequency Current Transformers as Partial Discharge Sensors for Underground Cables.*" IEEE Transactions on Dielectrics and Electrical Insulation, vol. 20, no. 3, *IEEE*, 2013, pp. 814–24.

[19] IEEE Standard for High-Voltage Switchgear (Above 1000 V) Test Techniques – Partial Discharge Measurements. IEEE, 2009, pp.1-72.

[20] Ahmed, N and N.Srinivas. "*On-Line Partial Discharge Detection in Cables*. " IEEE Transactions on Dielectrics and Electrical Insulation, vol. 5, no. 2, *IEEE*, 1998, pp. 181–88.

[21] Stastný, L., Mego, R., Pihera, J., & Hornak, J. (2020). "*Selectivity of inductive coupling for partial discharge measurement in MV cables*.", 2020 International Conference on Diagnostics in Electrical Engineering (Diagnostika), 1-4.

[22] Lundgaard, L. "*Partial Discharge. XIII. Acoustic Partial Discharge Detection-Fundamental Considerations.* " IEEE Electrical Insulation Magazine, vol. 8, no. 4, *IEEE*, 1992, pp. 25–31.

[23] Mohamed, F. P., *et al.* "*Partial Discharge Location in Power Cables Using a Double Ended Method Based on Time Triggering with GPS.*" IEEE Transactions on Dielectrics and Electrical Insulation, vol. 20, no. 6, *IEEE*, 2013, pp. 2212–21.

[24] Illias, H. A., *et al.* "*Comparison Between Three-Capacitance, Analytical-Based and Finite Element Analysis Partial Discharge Models in Condition Monitoring.* " IEEE Transactions on Dielectrics and Electrical Insulation, vol. 24, no. 1, *IEEE*, 2017, pp. 99–109.

[25] Danikas, M. *et al.* "*Discussion: Partial Discharges in Ellipsoidal and Spheroidal Voids.* " IEEE Transactions on Electrical Insulation, vol. 26, no. 3, *IEEE*, 1991, pp. 537–39.

[26] Pedersen, A., *et al.* "*The Theory and Measurement of Partial Discharge Transients.* " IEEE Transactions on Electrical Insulation, vol. 26, no. 3, *IEEE*, 1991, pp. 487–97.

[27] Callender, G., *et al.* "*Critical Analysis of Partial Discharge Dynamics in Air Filled Spherical Voids.* " *Journal of Physics. D*, Applied Physics, vol. 51, no. 12, IOP Publishing, 2018, p. 125601.

[28] Morsalin, S., *et al.* "*Measurement and Modeling of Partial Discharge Arising from Different Cavity Geometries at Very Low Frequency.* " IEEE Transactions on Dielectrics and Electrical Insulation, vol. 27, no. 4, *IEEE*, 2020, pp. 1110–18.

[29] Original Manual v1.4, Ultimaker 3 Installation and User Manual, 2017.

[30] Wolf and Associates, Airwolf 3D Axiom Dual Direct Drive Operation Guide, 2016.

[31] Béchet, E., *et al.* "*Generation of a Finite Element MESH from Stereolithography (STL) Files.* " Computer Aided Design, vol. 34, no. 1, Elsevier Ltd, 2002, pp. 1–17

[32] Digital instrument Vecco Meterology Group, Dimensions TM 3100 Manual, Version 4.43C, 2003.

[33] Vecco Instruments Inc, NanoScope Software 6.13 User Guide, Part Number 004 132000(standard) 004-132-100(cleanroom), 2004.

[34] Murthy, N. "*9 - Techniques for Analyzing Biomaterial Surface Structure, Morphology and Topography*. " Surface Modification of Biomaterials, Elsevier Ltd, 2011, pp. 232–55.

[35] Chao Yuan, *et al.* "*Dielectric Response Characterization of in-Service Aged Sheds of (U) HVDC Silicone Rubber Composite Insulators.* " IEEE Transactions on Dielectrics and Electrical Insulation, vol. 23, no. 3, *IEEE*, 2016, pp. 1418–26.

[36] SkyScan 1275, Bruker MicroCT 2016 User Manual V1.1, 2016

[37] Ohki, Y., and N. Hirai. "*Electrical Conduction and Breakdown Properties of Several Biodegradable Polymers.* " IEEE Transactions on Dielectrics and Electrical Insulation, vol. 14, no.6, *IEEE*, 2007, pp. 1559–66.

[38] Mantach, S., Gill, P., Oliver, D.R., Ashraf, A., & Kordi, B., "*An interpretable CNN model for classification of partial discharge waveforms in 3D-printed dielectric samples with different void sizes.* " Neural Computing & Applications, 2022.

Appendix A:

Relative Permittivity analysis of PLA sample

Relative permittivity of the PLA disc samples was measured using *the Solartron Analytical Modulab XM* dielectric spectroscope at an average of frequency over the range of 1 Hz to 10^5 Hz. The results from the experiment are presented in Table 4.2. The resulting values deviated from the expected literature value of 2.7 [36]. The variation in the result was believed to be due to the presence of the imperfections along the print lines in the PLA disc sample.

To confirm this assumption finite element simulations using *COMSOL Multiphysics* software were performed for air gap scenarios that had a track period of 350 µm and varying heights of 35 µm, 10 µm, and 3 µm. The largest of these heights corresponds to the largest feature observed during the sample characterization.

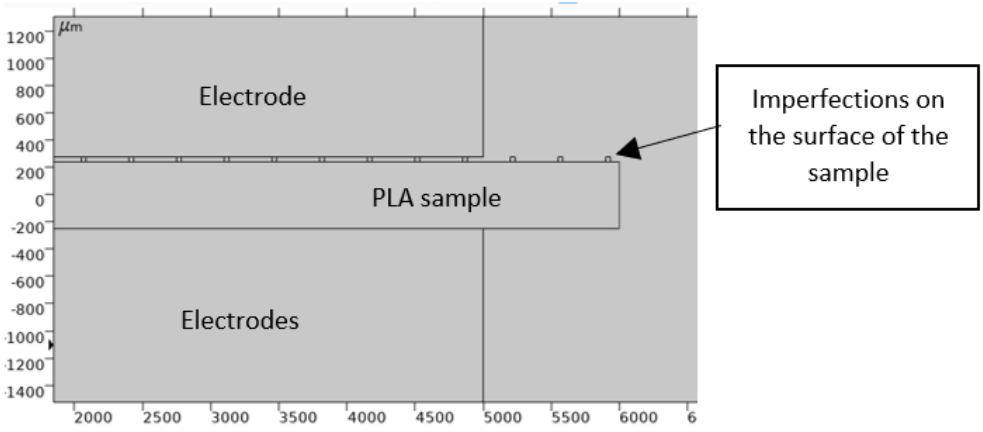

Figure A.1: Image from finite element simulation- cross section of electrodes in contact with PLA sample with imperfections at the surface of the sample.

Table A.1: Finite element analysis result form COMSOL Multiphysics simulation

Height of Imperfection (μm)	$\|\varepsilon_r\|$
35	1.93
10	2.12
3	2.18

With increased track height, the relative permittivity decreased. The range of relative permittivity values obtained for track heights in the range 3 μm - 35 μm correspond to the range of values obtained experimentally (able 4.2). This supports the hypothesis that the discrepancy between the experimental data and data available in literature was due to the presence of the imperfections at the surface due to the tracks created during the 3D printing of the PLA samples. It also confirms the importance of refining the 3D- printing process to minimise the size of these tracks (ensuring better contact between the electrode and the sample).

Appendix B:

Microtomography Analysis of PLA Samples

Multiple samples with different dimensions and printer settings were printed in the duration of the thesis. Each 3D printed sample was put under X-ray scans. Microtomography is a technique used to obtain three-dimensional image information of sample by producing 2D shadow images in x-ray that are reconstructed using an instrument *Bruker SKYSCAN 1272*. This technique of achieving reconstructed 3D images help in knowing the fabrication of 3D printed samples.

The first set of cylindrical 3D printed sample had void designed at the surface of the sample. These samples were printed to validate the fabrication process of printing sample with voids. The samples in this sample set had voids at the surface (hemisphere, cone, hollow cylinder, and solid cylinder).

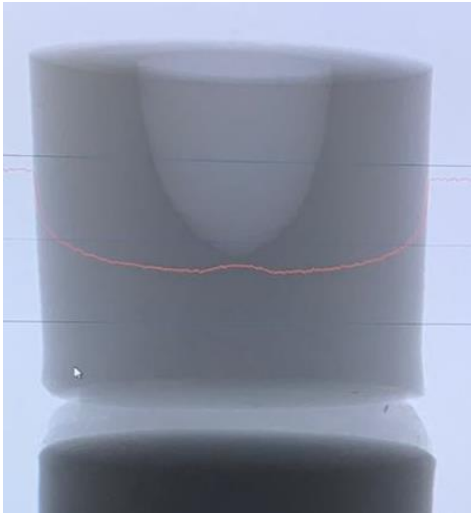

Figure B.1: X-ray shadow image of sample with a hemispherical void at the surface of the cylindrical sample.

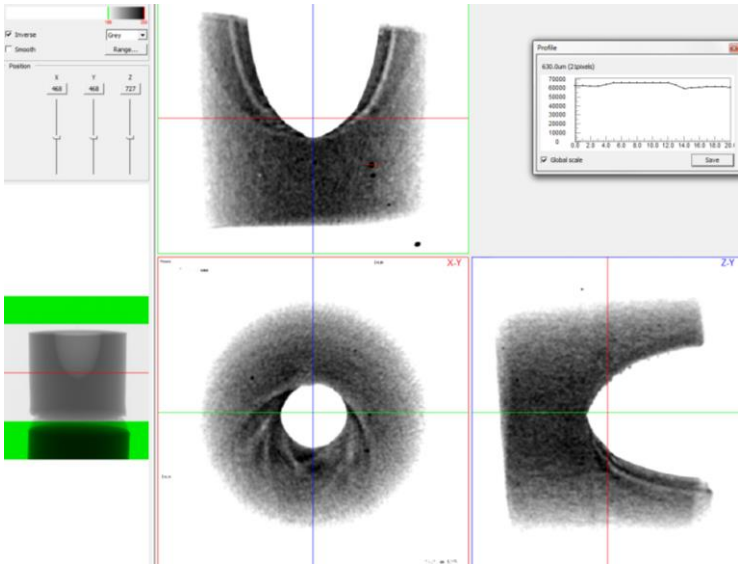

Figure B.2: Two-dimensional Image of cylindrical sample with hemispherical void at the surface along the X-Z, X-Y and Z-Y axis

The scans produced by this sample set gave confidence in the fabrication process confirming the shape and presence of the void in the sample. The next step was to determine the size of the void that could be designed at the center along the rotational axis of the sample.

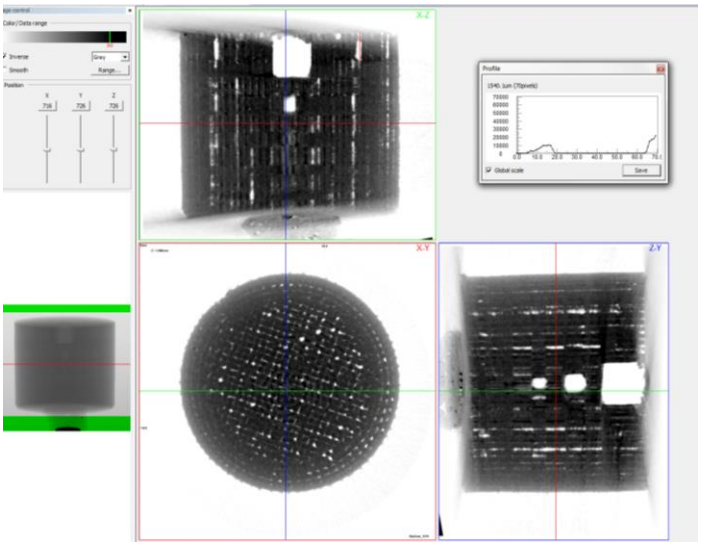

Figure B.3 Two-dimensional image of cylindrical sample with multiple voids of 2 mm, 1 mm, 0.75 mm, and 0.50 mm.

Analysing a sample with multiple voids showed the distortion in the shape of the designed void, along with many imperfections in the solid area. The imperfections were created during the printing along the print lines in the sample.

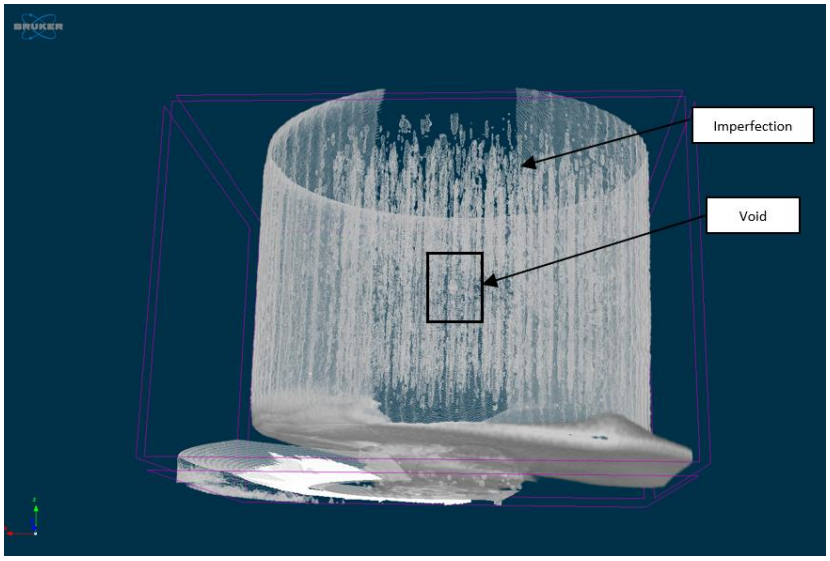

Figure B.4: Reconstructed three-dimensional image of the sample with a void at the center along the rotational axis of the cylinder.

The initial samples were printed at a flow rate of 90% and had numerous imperfections in the solid area. The next set of samples printed were at greater flow rates (97% and 98%) printer bed temperatures of 215 ℃ and 220 ℃.

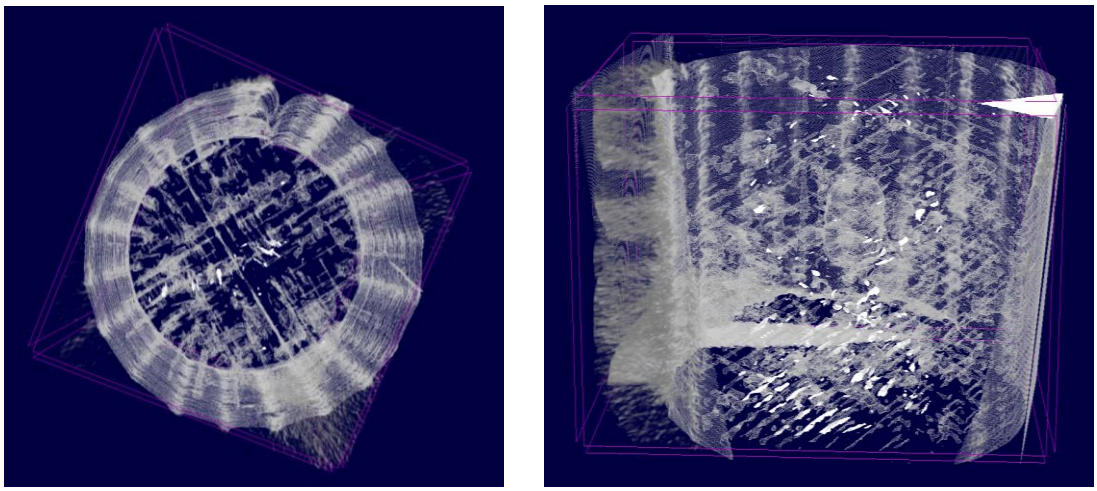

(a) (b)

Figure B.5. Reconstructed three dimensional of samples printed sample with 97% flow rate. (a) control sample with 12 mm (height and diameter) (b) Sample with a void of 2 mm (height and diameter) at the center along the axis of rotational symmetry

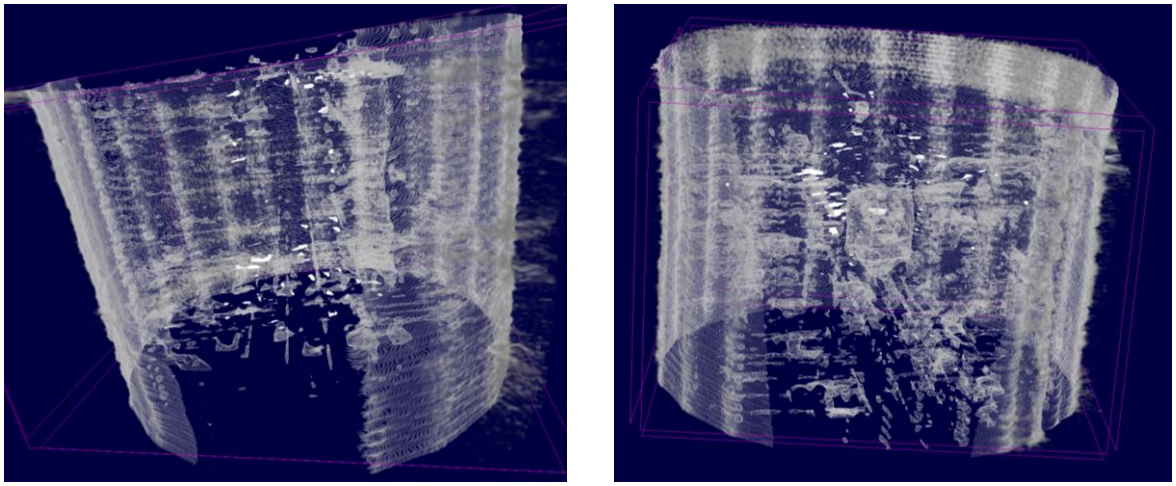

(a) (b)

Figure B.6. Reconstructed three dimensional of samples printed at 98% flow rate (a) Control sample with dimensions 12 mm (height and diameter) (b) Sample with 2 mm (height and diamter) void at the center.

The three dimensional x-ray scans of sample printed at a flow rate of 98% and 97% had fewer imperfections compared to the samples printed at a lower flow rate. The next set of samples (height:5 mm and diameter: 12 mm) were printed at 100% flow rate and a printer bed temperature at 220 °C.

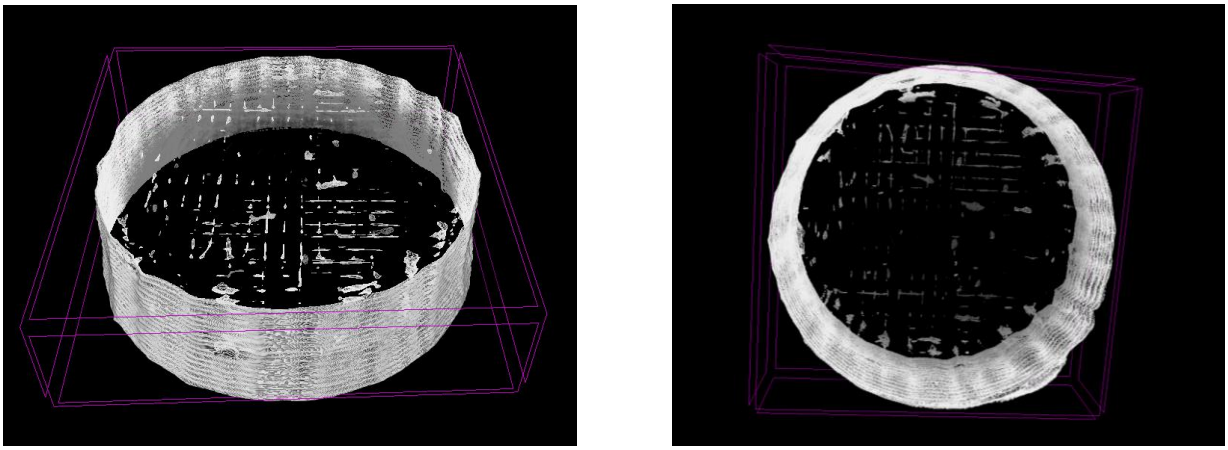

(a) (b)

Figure B.7: Reconstructed three dimensional image of a control sample with 5 mm height and 12 mm diameter (a) Top view of the sample showing imperfections near the surface. (b) Bottom view of the sample showing imperfections only in the upper layers of the sample.

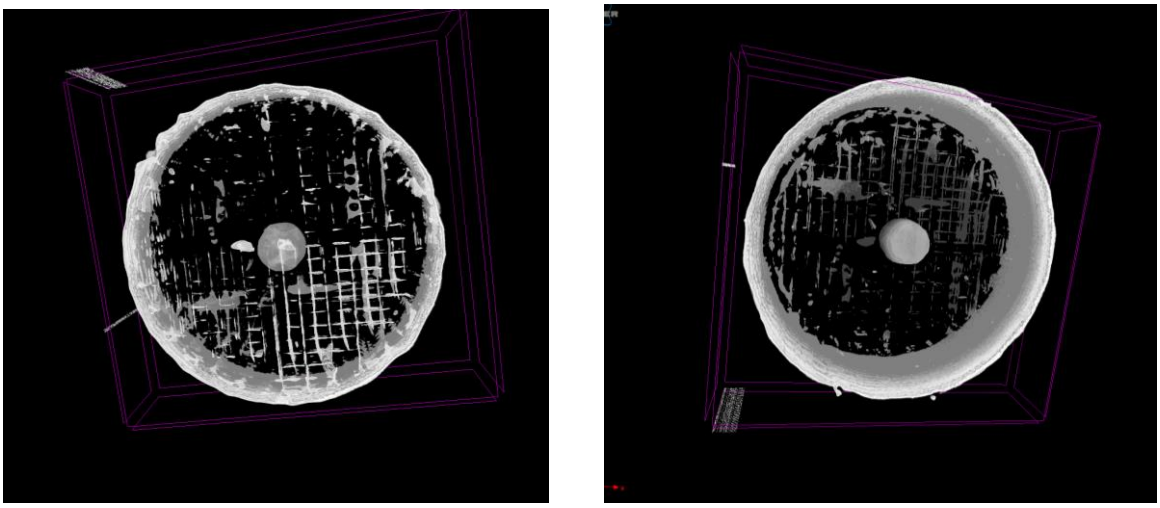

(a) (b)

Figure B.8: Reconstructed three dimensional image of a 5 mm (height and diameter) sample with single void 2 mm (height and diamter) (a) Top view of the sample showing imperfections and void at the center along the rotational axis of the cylindrical sample. (b) Bottom view of the sample showing imperfections only in the upper layers of the sample and the void at the center

Samples at 100% flow rate had fewer imperfections compared to the samples at a lower flow rate. Additionally, it was observed that the amount of imperfections in the sample increased as we move farther from the heated printer bed.

APPENDIX C:

Partial Discharge Measurement of the PLA Samples

Partial Discharge experiment were performed on multiple samples of different dimensions and voids. In accordance with the IEC 60270 standard. Phase resolved partial discharge patterns were observed when a 60 Hz voltage is applied to the high voltage electrodes with samples between them. The samples and electrodes are immersed in transformer oil to avoid any surface discharge. The observation from the experiments is summarized below.

Table C.1: Partial discharge measurements of samples.

Sample	Void Size	PDIV (kV)	PDEV (kV)	Highest Voltage (kV)	Comments (kV)
Height: 12 mm Diameter:12 mm	No void (control)	5.33	4.7	6.58	Strong disturbance in PRPD
Height: 12 mm Diameter:12 mm	Height: 2 mm Diameter:2 mm	No PD up to 14 kV			
Height: 12 mm Diameter:12 mm	Height: 0.5 mm Diameter:0.5 mm	7.369	7.33	7.99	
Height: 12 mm Diameter:12 mm	No void (control)	No PD up to 15 kV			
Height: 12 mm Diameter:12 mm	Height: 1 mm Diameter:1 mm	3.8	3.5	4.4	
Height: 12 mm Diameter:12 mm	Height: 2 mm Diameter: 2 mm	15.5			Accompanied by strong discharge and noise

Table C.1: Partial Discharge measurements of samples (continued).

Sample	Void Size	PDIV (kV)	PDEV (kV)	Highest Voltage (kV)	Comments (kV)
Height: 3 mm Diameter: 12 mm	No void	No PD up to 10kV			
Height: 3 mm Diameter: 12 mm	Height: 1 mm Diameter: 1 mm	4.60	4.47	5.52	
Height: 5 mm Diameter:12 mm	Height: 2 mm Diameter: 2 mm	3.70	3.70	4.50	
Height: 5 mm Diameter:12 mm	No void	4.985		6	Accompanied by a buzzing noise
Height: 12 mm Diameter:12 mm	Height:0.75 mm Diameter:0.75 mm	11.2	10.1	12.5	
Height: 5 mm Diameter:12 mm	Height: 2 mm Diameter: 2 mm	12.5	8.2	15	Extinction voltage is lower than inception voltage. The discharge voltage gradually decreases until completely gone at 8.2 kV
Height: 5 mm Diameter:12 mm	Height: 2 mm Diameter:2 mm	12	10.5	14.67	
Height: 5 mm Diameter:12 mm	Height: 2 mm Diameter:2 mm	2.4	2	2.8	
Height: 5 mm Diameter:12 mm	Height: 2 mm Diameter:2 mm	2.4	2	2.8	Sample was immersed in oil for 2 weeks
Height: 5 mm Diameter: 12 mm	No void (control)	No PD up to 17 kV			PD results are close to what is expected from control sample
Height: 5 mm Diameter: 12 mm	No void (control)	12	12	14	Magnitude of PD was low
Height: 20 mm Diameter:12 mm	Multiple Void samples- 2mm, 1mm,0.75mm, 0.50mm	19.64	20.58	23	

All the samples showed similar patterns of partial discharge in PRPD with some variations in the magnitude. The observations of two samples with similar dimensions are different. This confirms the presence of imperfections in the sample formed during the fabrication process.

APPENDIX D:

Profilometry results for the PLA samples

Profilometry was performed on disc samples and samples with voids at the surface of different shapes- square, triangle, circle, and ellipse (figure 3.8) using the *KLA- Tencor AlphaStep 500 (AS 500)* profiler. The aim of the experiment was to quantify the roughness of the PLA disc sample (before and after ironing), and the roughness of void in the sample. For the sample with voids the depth was measured relative the uppermost layer of the sample. Additionally, the profilometry scans gave a better understanding of the height of the print lines inside the voids.

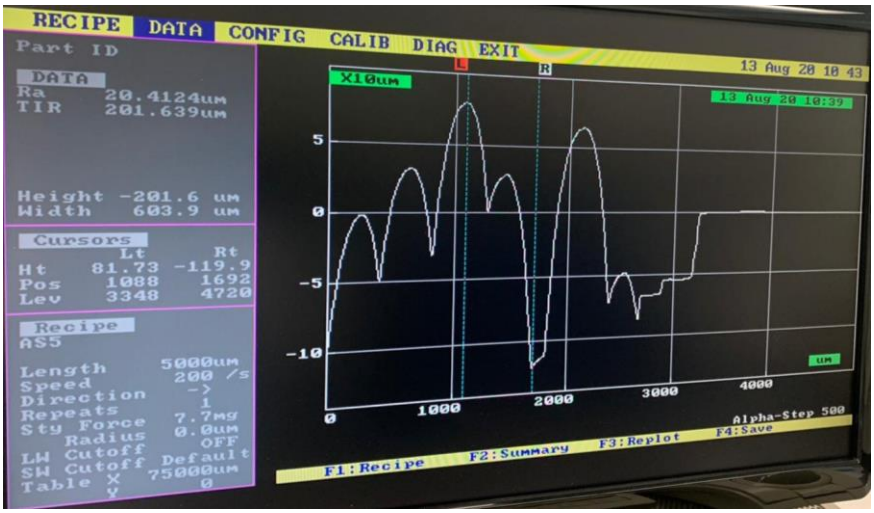

Figure D.1: Profilometry scan of the sample with square void (Figure 3.8) at the surface.

Figure D.2: Profilometry scan of the sample with circular void (Figure 3.8) at the surface.

Scans from all the samples showed variation (high-low peaks) while scanning inside the sample, confirming the roughness at the bottom of the voids due to the print lines. This roughness was similar to the roughness of the disc sample on the side away from the heated printer bed.